

# Structural characterization of kappa-opioid receptor dimer in complex with two G proteins

Received: 10 August 2025

Accepted: 13 May 2026

Cite this article as: Zhao, Y., Xu, C., Wang, Y. *et al.* Structural characterization of kappa-opioid receptor dimer in complex with two G proteins. *Nat Commun* (2026). <https://doi.org/10.1038/s41467-026-73615-x>

Yuxi Zhao, Chanjuan Xu, Yue Wang, Hong Shan, Jing Wang, Yuxuan Liu, Xin Luo, Junrui Li, Mingyang Li, Yini Liu, Kai Wu, Bryan L. Roth, Xi-Ping Huang, H. Eric Xu, Jianfeng Liu & Youwen Zhuang

We are providing an unedited version of this manuscript to give early access to its findings. Before final publication, the manuscript will undergo further editing. Please note there may be errors present which affect the content, and all legal disclaimers apply.

If this paper is publishing under a Transparent Peer Review model then Peer Review reports will publish with the final article.

---

## Structural characterization of kappa-opioid receptor dimer in complex with two G proteins

Yuxi Zhao<sup>1,2,#</sup>, Chanjuan Xu<sup>3,#</sup>, Yue Wang<sup>1,#</sup>, Hong Shan<sup>1</sup>, Jing Wang<sup>4</sup>, Yuxuan Liu<sup>3</sup>, Xin Luo<sup>3</sup>, Junrui Li<sup>1</sup>, Mingyang Li<sup>5,6,7</sup>, Yini Liu<sup>5</sup>, Kai Wu<sup>1,8</sup>, Bryan L. Roth<sup>4</sup>, Xi-Ping Huang<sup>4</sup>, H. Eric Xu<sup>1,2,9,\*</sup>, Jianfeng Liu<sup>3,\*</sup>, Youwen Zhuang<sup>5,6,7,\*</sup>

<sup>1</sup> State Key Laboratory of Drug Research. Center for Structure and Function of Drug Targets, Shanghai Institute of Materia Medica, Chinese Academy of Sciences, Shanghai 201203, China

<sup>2</sup>School of Chinese Materia Medica, Nanjing University of Chinese Medicine, Nanjing 210023, China

<sup>3</sup>Cellular Signaling laboratory, International Research Center for Sensory Biology and Technology of MOST, Key Laboratory of Molecular Biophysics of MOE, College of Life Science and Technology, Huazhong University of Science and Technology, Wuhan, Hubei 430074, China

<sup>4</sup>Department of Pharmacology, University of North Carolina at Chapel Hill School of Medicine, Chapel Hill, NC 27599, USA

<sup>5</sup>Department of Pharmaceutical and Artificial-Intelligence Sciences, School of Medicine, Shanghai Jiao Tong University, Shanghai 200025, China

<sup>6</sup>Artificial Intelligence Clinical Research Center for drug discovery, Shanghai Key Laboratory of Flexible Medical Robotics, Tongren Hospital, School of Medicine, Shanghai Jiao Tong University, Shanghai 200025, China

<sup>7</sup>Key Laboratory of Cell Differentiation and Apoptosis of Chinese Ministry of Education, School of Medicine, Shanghai Jiao Tong University, Shanghai 200025, China

<sup>8</sup>The Shanghai Advanced Electron Microscope Center, Shanghai Institute of Materia Medica, Chinese Academy of Sciences, Shanghai 201203, China

<sup>9</sup>University of Chinese Academy of Sciences, Beijing 100049, China

#These authors contributed equally to this paper.

\*Correspondence: H. Eric Xu ([eric.xu@simm.ac.cn](mailto:eric.xu@simm.ac.cn)), Jianfeng Liu ([jfliu@mail.hust.edu.cn](mailto:jfliu@mail.hust.edu.cn)) or Youwen Zhuang ([youwen\\_zhuang@sjtu.edu.cn](mailto:youwen_zhuang@sjtu.edu.cn))

ARTICLE IN PRESS

**Abstract**

The  $\kappa$ -opioid receptor ( $\kappa$ OR) represents a promising non-addictive analgesic target due to its critical role in pain and reward pathways. Despite evidence of  $\kappa$ OR dimerization, its molecular basis and pharmacological significance remain elusive. Here, we demonstrate stable  $\kappa$ OR dimer formation in living cells and present cryo-electron microscopy structures of salvinorin A-bound  $\kappa$ OR dimer complexed with two  $G_i$  proteins, revealing a parallel assembly distinct from previously characterized GPCR dimers that engage only single G protein. Multiple membrane lipids are positioned at the TM1-Helix 8 interface, where they make extensive contacts with both protomers and may contribute to the stability of the  $\kappa$ OR dimer. Importantly, dimerization significantly enhances  $G_i$  protein recruitment to  $\kappa$ OR in both potency and efficacy. We also demonstrate that salvinorin A, a non-nitrogenous agonist, binds similarly in monomeric and dimeric  $\kappa$ OR, and identify Y312<sup>7,35</sup> as a critical selectivity determinant across opioid receptors. These findings expand our understanding of opioid receptor pharmacology and signaling, providing a foundation for developing superior  $\kappa$ OR-targeted therapeutics for pain and related disorders.

## Introduction

Effective and safe pain management continues to be a significant challenge in current health care. Opioids are currently the most widely used and effective analgesic medications. Opioid drugs such as morphine and fentanyl continue to be the primary treatments for moderate to severe pain, exerting their analgesic effects by targeting opioid receptors (ORs). The OR family includes four receptor types, namely  $\mu$ OR,  $\delta$ OR,  $\kappa$ OR, and NOPR, all of which primarily couple to the inhibitory  $G_{i/o}$  protein<sup>1</sup>. Currently, most approved opioid analgesics are  $\mu$ OR agonists, offering potent pain relief but accompanied by significant adverse effects, particularly addiction and respiratory depression, which greatly limit their clinical utility. The fatal respiratory depression resulting from opioid addiction has directly fueled the widespread “opioid crisis”, particularly in North America, claiming about 100,000 lives annually<sup>2</sup>. The  $\kappa$ OR has emerged as a promising alternative therapeutic target for pain modulation, offering potential benefits without the severe side effects associated with  $\mu$ OR agonists<sup>3, 4, 5</sup>.

Understanding the intricate signaling and pharmacological properties of ORs is crucial for developing effective analgesics with fewer side effects<sup>5, 6</sup>. The molecular understanding of  $\kappa$ OR has advanced considerably since its initial cloning, driven by its therapeutic potential for analgesia and anhedonia<sup>7, 8</sup>. Structural studies have illuminated the receptor’s inactive and active conformations, providing valuable insights into ligand interactions and signaling dynamics<sup>9, 10, 11, 12, 13, 14</sup>. Elucidation of  $\kappa$ OR bound to the antagonist JD1c has facilitated the development of therapies for depression-related anhedonia, exemplified by the clinical advancement of navacprant<sup>15, 16</sup>. Furthermore, investigations of agonist-bound structures have illuminated the molecular basis of signaling bias, particularly how specific ligand interactions influence arrestin recruitment and G-protein coupling<sup>10, 11, 12, 13, 14</sup>. These structural insights, combined with our understanding of dynorphin recognition and G-protein coupling specificity<sup>13</sup>, have accelerated the rational drug design targeting  $\kappa$ OR for pain, pruritus, and affective disorders<sup>17</sup>.

The paradigm of GPCR function has evolved substantially with the recognition that these receptors can form functional dimeric and oligomeric complexes<sup>18, 19, 20</sup>. While traditionally viewed as monomeric entities, compelling evidence indicates that ORs can exist as both homo- and heterodimers, each exhibiting distinct functional properties<sup>21, 22, 23, 24, 25</sup>.  $\kappa$ OR presents a particularly intriguing case for studying receptor oligomerization, as it exhibits a remarkably high propensity for dimerization compared to other OR subtypes<sup>26</sup>. The temporal and spatial dynamics of  $\kappa$ OR dimerization in cellular membranes have been characterized<sup>26, 27</sup>. Advanced biophysical approaches including single-molecule imaging and split GFP complementation have revealed that  $\kappa$ OR spontaneously forms stable dimers at physiological expression levels, even at low receptor densities where  $\mu$ OR and  $\delta$ OR predominantly remain monomeric<sup>26</sup>. Quantitative analyses further support this observation, demonstrating significantly higher dimerization affinities for  $\kappa$ OR compared to  $\mu$ OR and  $\delta$ OR<sup>25</sup>. Despite these compelling observations of dimerization properties of  $\kappa$ OR, the molecular architecture governing dimer assembly and the functional consequences of this oligomerization remain undefined.

In this study, we provide direct evidence for stable  $\kappa$ OR dimerization in cell membranes. We also present structural snapshots of the  $\kappa$ OR dimer captured during our investigation of the  $\kappa$ OR- $G_i$  signaling complexes bound to the natural product agonist, salvinorin A (SalA). Through complementary approaches combining NanoBiT protein interaction assays, site-directed cysteine cross-linking, and functional  $G_i$  dissociation measurements, we characterize the lipid-mediated dimer interface and demonstrate that dimerization significantly enhances  $G_i$ -mediated signaling efficacy. These findings provide molecular-level insights into  $\kappa$ OR oligomerization and its functional consequences, establishing a foundation for development of improved analgesics targeting  $\kappa$ OR signaling.

## Results

### Stable dimerization of $\kappa$ OR in living cells

We firstly employed the bimolecular fluorescence complementation (BiFC) assay to examine  $\kappa$ OR dimerization in living cells (**Fig. 1**). Two  $\kappa$ OR constructs were generated, one fused to VN and the other fused to VC at their C-terminus, allowing visualization of  $\kappa$ OR dimerization through Venus complementation (**Fig. 1a**). As expected, cells expressing  $\kappa$ OR-VN or  $\kappa$ OR-VC alone produced no detectable fluorescent signal, confirming that neither fragment independently reconstitutes a functional Venus protein. In contrast, co-transfection of <sup>FLAG</sup> $\kappa$ OR-VN and <sup>FLAG</sup> $\kappa$ OR-VC yielded a strong fluorescent signal, indicating the formation of  $\kappa$ OR dimer (**Fig. 1b-d**). To verify the specificity of this interaction, we introduced a third untagged receptor through competitive displacement. Co-transfection of <sup>HA-snap</sup> $\kappa$ OR substantially reduced BiFC fluorescence, consistent with competition for dimerization partners. Importantly, neither the <sup>snap</sup>GB2 (a GABA<sub>B</sub> receptor subunit that can't function alone and doesn't interact with  $\kappa$ OR) nor CAAX-mCherry (a membrane-anchored marker) significantly altered fluorescence intensity, together indicating the specific dimer formation between  $\kappa$ OR-VN and  $\kappa$ OR-VC (**Supplementary Fig. 1a-b**). These findings provide further evidence for the existence of  $\kappa$ OR dimers at the cellular membranes, corroborating observations from previous studies<sup>23, 24, 26</sup>. Then, we used NanoBiT complementation assay to investigate if agonist ligands modulate  $\kappa$ OR dimerization. To this end, two  $\kappa$ OR constructs were generated, one fused with the large subunit (LgBiT) and the other with the small subunit (SmBiT) of the NanoBiT system at their C-terminus, allowing luminescence complementation to report  $\kappa$ OR- $\kappa$ OR association (**Fig. 1e**). Treatment with a panel of  $\kappa$ OR agonists, including 6'-GNT1, U -69593, CR845 and dynorphin A<sub>1-13</sub>, showed no significant influence on dimer formation. Nalfurafine and SalA slightly decreased dimer formation. Notably, none of the agonists tested completely disrupted  $\kappa$ OR dimer formation (**Fig. 1e**), suggesting a stable  $\kappa$ OR dimerization.

### Structure of dimeric $\kappa$ OR-G<sub>i</sub> signaling complex

To elucidate the molecular mechanism underlying  $\kappa$ OR dimer formation and G protein signaling, we sought to obtain and characterize the structure of the dimerized  $\kappa$ OR-G<sub>i</sub> signaling complex. We

selected the non-nitrogenous neoclerodane SalA as the orthosteric ligand. The SalA-bound  $\kappa$ OR- $G_i$  complex was assembled and purified for cryo-electron microscopy (cryo-EM) analysis through co-expression of  $\kappa$ OR with the  $G_i$  heterotrimer (**Supplementary Fig. 2a-b**). During purification, we observed two adjacent peaks of the  $\kappa$ OR- $G_i$  complexes, which were collected for subsequent structural investigation. Single-molecule mass photometry performed on the affinity-purified sample prior to any concentration or SEC fractionation revealed three discrete populations corresponding to detergent micelles, monomeric  $\kappa$ OR- $G_i$  complex, and a dimeric  $\kappa$ OR- $G_i$  species, with the latter two exhibiting an ~1:2 mass relationship (**Supplementary Fig. 2a**). These findings support that the 2:2  $\kappa$ OR- $G_i$  dimer pre-exists in dilute detergent solution. Although the protein complex predominantly assembled in a monomeric state, 3D classification of single particles identified a distinct class of  $\kappa$ OR- $G_i$  dimers, enabling structural determination of the dimeric  $\kappa$ OR- $G_i$  signaling complex (**Supplementary Fig. 2c-d and Supplementary Table 1**). The SalA-bound  $\kappa$ OR- $G_i$  monomer and dimer density maps were resolved with overall resolution at 3.2 Å and 3.6 Å, respectively. For the dimeric complex, refinement was performed with C2 symmetry, consistent with the two-fold arrangement observed in the reconstruction. Imposing C2 symmetry improved the global and local map quality relative to C1 refinement, and the C2-symmetrized map was therefore used for model building and analysis. To aid interpretation, we produced both a conventionally post-processed map and a DeepEMhancer-processed map from the same C2-refined particle set; these complementary representations were examined in parallel, as DeepEMhancer preferentially enhances continuous protein features whereas conventional post-processing more consistently preserves certain membrane-proximal, non-protein densities. The cryo-EM maps allowed unambiguous modeling of side chains for  $\kappa$ OR, SalA, lipids and most of the  $G_i$  heterotrimer (**Supplementary Fig. 3**). However, because the  $G_i$  density is locally weaker in the dimer reconstruction,  $G_i$  was modeled by fitting the validated monomeric  $\kappa$ OR- $G_i$  structure into the available density followed by manual inspection (**Figs. 2a-c and Supplementary Fig. 2e**). Notably, our  $\kappa$ OR- $G_i$  dimer structure shows that each  $\kappa$ OR protomer couples to one  $G_i$  protein (2:2 stoichiometry) in a parallel arrangement. This mode of assembly differs markedly from previously

reported dimeric GPCR-G-protein complexes. The class D fungal receptor Ste2 also forms a 2:2 receptor-G-protein complex, but its dimer interface is generated primarily by the N terminus, ECL1, TM1, TM2, and TM7 in a domain-swapped configuration, featuring a right-handed TM1-TM1 crossing angle of  $\sim 37^\circ$  and an extensive protein-protein interface<sup>28, 29</sup>. In contrast, the  $\kappa$ OR dimer interface is mediated predominantly by TM1 and Helix 8, assisted by interfacial lipids, resulting in a distinct TM1-TM1 packing geometry while still accommodating two  $G_i$  heterotrimers on the intracellular side (**Figs. 2a-b**). Together with the previously reported structures of apelin receptor (APJ)<sup>30, 31</sup>, GPR3<sup>32</sup> and class C GPCR dimer exhibiting a 2:1 receptor-G protein stoichiometry<sup>33, 34</sup>, these comparisons indicate that the  $\kappa$ OR- $G_i$  homodimer complex represents a distinct structural arrangement for coupling two G proteins to a class A GPCR dimer.

### **Binding mode of SalA in $\kappa$ OR**

SalA is a naturally occurring diterpenoid that represents the principal psychoactive constituent of *Salvia divinorum*. In contrast to classical hallucinogens which primarily target serotonergic receptors, SalA stands out as a selective and potent agonist at  $\kappa$ OR, with nanomolar binding affinity<sup>35</sup>. Unlike traditional OR ligands, SalA lacks a basic nitrogen atom, a feature previously considered a prerequisite for OR interaction. Its complex molecular architectures, characterized by a distinctive tricyclic core scaffold with a furan ring and multiple stereocenters, underpins its marked affinity and specificity for  $\kappa$ OR.

Structural analysis revealed high conformational conservation between the monomeric and dimeric states of SalA-bound  $\kappa$ OR, with minimal deviation in receptor backbone (RMSD = 0.35 Å) and ligand positioning (**Supplementary Fig. 4**). To elucidate precise ligand-receptor interactions, we utilized the higher-resolution monomeric structure. In this configuration, SalA occupied the orthosteric binding pocket (OBP), with its tricyclic diterpenoid core vertically inserting into the conserved chamber of ORs, a region typically occupied by the conserved “YGGF” motif found in endogenous opioid peptides<sup>13</sup>. This chamber was suggested to be critical for the

recognition and activation of ORs by their ligands<sup>13</sup>. Comparative structural analyses of  $\kappa$ OR bound to SalA and other opioid ligands, such as MP1104 and nalfurafine, reveal a highly congruent binding pose despite their chemical diversity<sup>10, 12</sup> (**Fig. 2d**). SalA establishes extensive interactions with key residues from TM2-3, and TM5-7 of  $\kappa$ OR, facilitating robust receptor activation (**Fig. 2e**).

The negatively charged residue D<sup>3.32</sup> (Ballesteros-Weinstein numbering rules<sup>36</sup>) is highly conserved among ORs and aminergic receptors, where it typically forms a salt bridge with the ligand's amino group, anchoring the ligand to the OBP and facilitating receptor activation<sup>37, 38, 39</sup>. Although SalA lacks amino group, the carbonyl oxygen of its terpenoid ring and acetyloxy moiety establish extensive hydrogen-bond interactions with D138<sup>3.32</sup> and Q115<sup>2.60</sup> (**Fig. 2f**). These interactions are further reinforced by hydrogen bonds with Y320<sup>7.43</sup>, forming a polar network that compensates for the absence of an amino group in conventional opioid ligands. Consistently, mutational studies substituting D138<sup>3.32</sup> or Q115<sup>2.60</sup> with alanine reduced the potency of SalA 10~26 fold at  $\kappa$ OR (**Fig. 2g**). In addition to polar interactions, SalA engages in extensive hydrophobic interactions within the OBP of  $\kappa$ OR. The diterpenoid core of SalA is sandwiched by residues from TM3 and TM7, together with the carboxylate ester moiety, interacts hydrophobically with Y139<sup>3.33</sup>, M142<sup>3.36</sup>, I290<sup>6.51</sup>, H291<sup>6.52</sup>, I294<sup>6.55</sup>, Y312<sup>7.35</sup>, and I316<sup>7.39</sup> (**Fig. 2h**). Alanine mutations of these residues, with the exception of I294<sup>6.55</sup>A, attenuated the potency of SalA on  $\kappa$ OR by more than 10-fold (**Fig. 2g-i and Supplementary Table 2**), suggesting the critical role of these hydrophobic packing in SalA-mediated  $\kappa$ OR activation. The preserved potency of I294<sup>6.55</sup>A suggests that the contribution of this residue may be functionally compensated by neighboring hydrophobic contacts within the pocket. The furan ring of SalA points toward the cleft of TM2 and TM3, occupying an extended hydrophobic pocket comprising W124<sup>ECL1</sup>, V134<sup>3.28</sup>, and I135<sup>3.29</sup>. This positioning mirrors the binding modes of the furan ring in nalfurafine<sup>12</sup>, the iodobenzene ring in MP1104, and the phenylalanine residue in dynorphin<sup>13</sup> (**Fig. 2j**). Consistently, mutations of V134<sup>3.28</sup> and I135<sup>3.29</sup> on  $\kappa$ OR decreased the EC<sub>50</sub> of SalA by 3-fold and 62-fold, respectively (**Fig.**

**2g and Supplementary Table 2**). In addition, the acetyloxy group of SalA extends downwardly to the intracellular side and was encapsulated within a hydrophobic network formed by V108<sup>2,53</sup>, W287<sup>6,48</sup> and Y320<sup>7,43</sup> (**Fig. 2k**), as occupied by the cyclopropylmethyl group of nalfurafine and MP1104. The encapsulation of the acetyloxy group within this hydrophobic environment enhances the stability of SalA's binding conformation, further contributing to receptor activation.

A prior docking and molecular dynamics study proposed a distinct SalA binding orientation in  $\kappa$ OR, placing the ligand above the morphinan binding region with the furan group oriented toward the intracellular core and the C2-acetoxy group directed toward ECL2<sup>40</sup>. In contrast, our cryo-EM structure reveals an inverted binding orientation in the signaling-competent  $\kappa$ OR-G<sub>i</sub> complex, in which the furan ring occupies an extracellular TM2-TM3 hydrophobic subpocket and the C2-acetoxy group extends toward the intracellular side where it is stabilized by TM2/3/6/7 residues (**Supplementary Fig. 5a**). Notably, this experimentally observed pose is consistent with the independently determined cryo-EM structure of  $\kappa$ OR bound to the salvinorin analogue momSalB<sup>11</sup> (**Supplementary Fig. 5b**), supporting a unified binding mode for salvinorin-type agonists.

### Selective determinants of SalA to ORs

To reveal how SalA conducts ligand selectivity toward  $\kappa$ OR over the OR family, we evaluated the activation profiles of SalA for the four ORs using the cell-based cAMP inhibition and  $\beta$ -arrestin1 recruitment assays (**Supplementary Fig. 6a-b**). We used DAMGO, Leu-enkephalin, dynorphin A<sub>1-13</sub> and nociceptin (NFQ) as the reference agonists for  $\mu$ OR,  $\delta$ OR,  $\kappa$ OR and NOPR, respectively. Consistent with previous studies, our findings demonstrated that SalA exhibits preferential activation of  $\kappa$ OR compared to other ORs in the G<sub>i</sub>-mediated cAMP inhibition pathway (**Supplementary Fig. 6a**). Notably, SalA displayed complete selectivity in  $\beta$ -arrestin1 recruitment, activating this pathway exclusively in  $\kappa$ OR while showing no detectable activity at  $\mu$ OR,  $\delta$ OR, or NOPR (**Supplementary Fig. 6b**). Structure superposition of SalA-bound  $\kappa$ OR with the other OR subtypes in their active states indicated that most residues interact with SalA are conserved, except

for the residue in 7.35 position (**Supplementary Fig. 6c**). In the SalA- $\kappa$ OR complex, the diterpenoid group of SalA forms Van der Waals forces and weak polar interaction with Y312<sup>7.35</sup> of  $\kappa$ OR, whereas the corresponding interactions are absent in the corresponding positions occupied by W320<sup>7.35</sup> in  $\mu$ OR, L300<sup>7.35</sup> in  $\delta$ OR, and L301<sup>7.35</sup> in NOPR. Supporting this observation, substitution mutations introducing tyrosine at position 7.35 in  $\mu$ OR,  $\delta$ OR, and NOPR enhanced SalA potency by approximately 5-10 folds (**Supplementary Fig. 6d-g**). Conversely, mutation of Y312<sup>7.35</sup> in  $\kappa$ OR to either tryptophan or leucine reduced SalA potency by 10 folds without significantly affecting dynorphin A<sub>1-13</sub> activity (**Supplementary Fig. 6g**). These findings identify Y312<sup>7.35</sup> as a critical determinant of the selective recognition of SalA to  $\kappa$ OR relative to other OR subtypes.

In complementary  $\beta$ -arrestin recruitment assays, we observed that although SalA robustly promotes  $\beta$ -arrestin1 recruitment at  $\kappa$ OR, it elicits a reduced maximal response for  $\beta$ -arrestin2 recruitment compared with dynorphin A<sub>1-13</sub> (**Supplementary Fig. 7**). Given the established dominant role of  $\beta$ -arrestin2 in GPCR desensitization and receptor internalization, this subtype-selective arrestin engagement provides a mechanistic explanation for the previously reported reduction in  $\kappa$ OR internalization following SalA stimulation relative to peptide agonists<sup>41</sup>. Together, these results indicate that SalA displays a distinctive signaling profile at  $\kappa$ OR, characterized by robust G<sub>i</sub> activation and preferential  $\beta$ -arrestin1 engagement, while limiting  $\beta$ -arrestin2-dependent regulatory processes.

### **Interfacial lipids contribute to $\kappa$ OR dimer stabilization**

In addition to the monomeric structure, we also resolved the structure of the dimeric SalA-bound  $\kappa$ OR-G<sub>i</sub> signaling complex with parallel receptor assembly. Structural analysis revealed that the  $\kappa$ OR dimer interface is mediated primarily by interactions between TM1 and Helix 8, similar to the architecture observed in several previously reported GPCR dimers (PDBs: 4DJH<sup>9</sup>, 4GPO<sup>42</sup>, and 6OFJ<sup>42</sup>; **Supplementary Figs. 4a-f**). Quantitative comparison of buried surface areas

calculated using PDBePISA demonstrates that the  $\kappa$ OR-G<sub>i</sub> dimer interface in our cryo-EM structure is substantially smaller (469 Å<sup>2</sup>) than those of the inactive  $\kappa$ OR crystal structure (1025 Å<sup>2</sup>)<sup>9</sup>, rhodopsin dimer (672 Å<sup>2</sup>)<sup>42</sup>, and the inactive state  $\beta_1$ -adrenergic receptor ( $\beta_1$ AR) dimer (834 Å<sup>2</sup>)<sup>43, 44</sup> (**Supplementary Fig. 8a-f**). For reference, the class D Ste2 receptor forms a domain-swapped dimer with a considerably larger interface (2467 Å<sup>2</sup>), though this represents a structurally distinct dimerization mechanism<sup>28</sup>. These results demonstrate that the active  $\kappa$ OR dimer interface is substantially smaller than all previously reported GPCR dimers that assemble through a TM1-TM1 interface, while still being larger than the TM3-ECL1-mediated interface of the APJ dimer (270 Å<sup>2</sup>)<sup>30, 31</sup> (**Supplementary Fig. 8g**). The reduced buried surface area in the active  $\kappa$ OR dimer is consistent with the limited set of hydrophobic contacts contributed primarily by V71<sup>1,44</sup>, V75<sup>1,48</sup>, F341<sup>8,54</sup>, and F346<sup>8,59</sup>. Notably, the cryo-EM map of the  $\kappa$ OR dimer revealed multiple well-defined lipid-like densities surrounding the receptor components, with a predominant distribution at the dimer interface (**Fig. 3a**). These observations suggest that membrane lipids could play a significant role in stabilizing the  $\kappa$ OR dimer. In these regions, the density is dominated by continuous hydrophobic features consistent with ordered acyl chains and sterol scaffolds, whereas reproducible density for polar headgroups is not observed, limiting confident assignment of specific phospholipid species. Accordingly, we modeled two C16:0 fatty acids (palmitic lipid molecule, PLM), twelve cholesterol (CLR) molecules and four cholesteryl hemisuccinate (CHS) molecules encircling the  $\kappa$ OR dimer (**Fig. 3b**), with the sterol-like features assigned as cholesterol or CHS based on the density features and sterol-containing purification conditions. We note, however, that cholesterol and CHS cannot always be unambiguously distinguished at this resolution, as the hemisuccinate moiety of CHS may be disordered and therefore not resolved. Thus, the densities modeled as cholesterol may also correspond to CHS with a disordered hemisuccinate group.

To comprehensively evaluate interactions across the entire interface, we employed the NanoBIT-based titration assay (**Fig. 3c**), a methodology previously validated for detecting noradrenaline

transporter dimerization<sup>45</sup>. To prevent signal artifacts from receptor overexpression, we maintained a constant transfection amount of LgBiT-κOR (500 ng) while incrementally increasing SmBiT-κOR plasmid concentrations to generate a dose-dependent NanoBiT signal curve. Based on our structural analysis showing that κOR dimer formation is mediated through residues from TM1, TM2, TM7, and Helix 8 directly or indirectly by membrane lipids (**Fig. 3b**), we analyzed the interface as two distinct regions: an extracellular component comprising TM1 and TM2 residues, and an intracellular component encompassing residues from TM1, TM7, and Helix 8. Within the extracellular interface region, CLR and CHS molecules occupy the interstitial space between protomers, establishing hydrophobic interactions with residues V60<sup>1.33</sup>, T63<sup>1.36</sup>, F70<sup>1.43</sup>, V71<sup>1.44</sup>, L74<sup>1.47</sup>, T117<sup>2.62</sup>, L120<sup>2.65</sup>, M121<sup>2.66</sup>, P125<sup>ECL1</sup>, and F126<sup>ECL1</sup> (**Fig. 3d-g**). The intracellular interface is similarly stabilized by two PLM and two CLR molecules, interacting with residues possessing predominantly bulky side chains such as L79<sup>1.52</sup>, F82<sup>1.55</sup>, F332<sup>7.55</sup>, and F344<sup>8.57</sup> (**Fig. 3g**). To evaluate the functional significance of these interactions, we conducted alanine substitution mutagenesis of all these residues, assessing dimer formation through titration experiments with fixed wild-type (WT) LgBiT-κOR against increasing concentrations of mutant SmBiT-κOR. Importantly, flow-cytometry analysis of cell-surface expression confirmed that none of the interface mutations reduced receptor expression or plasma-membrane localization relative to WT κOR (**Supplementary Fig. 9a and Supplementary Table 3**), ensuring that differences observed in the NanoBiT titration assays reflect altered dimerization rather than expression effects. Among the residues that make direct protomer-protomer contacts in the cryo-EM structure (V71<sup>1.44</sup>, V75<sup>1.48</sup>, F341<sup>8.54</sup>, and F346<sup>8.59</sup>), alanine substitutions at V75<sup>1.48</sup> and F341<sup>8.54</sup> produced the most pronounced effects, requiring ~1.5-fold and ~1.7-fold higher SmBiT-κOR plasmid amounts, respectively, to achieve dimerization levels comparable to WT (**Fig. 3d-g and Supplementary Table 3**). In contrast, mutations at other interface positions, many of which primarily contact interfacial lipids rather than the opposing protomer, did not significantly reduce dimerization and in some cases modestly increased the apparent dimerization propensity. These results indicate that a limited set of hydrophobic residues forming direct protein-protein contacts contributes

measurably to  $\kappa$ OR dimer stabilization, whereas interfacial lipids likely act as dynamic molecular fillers that accommodate subtle changes in side-chain packing rather than relying on specific lipid-contacting residues for dimer formation. To further exclude the possibility that the observed titration shifts arise from altered ligand responsiveness rather than changes in receptor-receptor association, we evaluated the ligand dependence of the NanoBiT readout. Full titration analyses using SalA, the endogenous agonist dynorphin A<sub>1-13</sub>, and the antagonist JD<sub>Tic</sub> showed comparable maximal NanoBiT signals and apparent EC<sub>50</sub> values for WT, V75<sup>1.48</sup>A, and F341<sup>8.54</sup>A receptors (**Supplementary Fig. 9b**), indicating that these mutations do not impair ligand recognition or overall receptor functionality. Thus, the rightward shifts observed in selected mutants reflect reduced  $\kappa$ OR- $\kappa$ OR association efficiency rather than altered pharmacological properties.

To directly examine whether membrane cholesterol functionally contributes to  $\kappa$ OR dimer stabilization, we manipulated cellular cholesterol levels using methyl- $\beta$ -cyclodextrin (M $\beta$ CD), a well-established reagent for acute cholesterol depletion. Cells co-expressing LgBiT- $\kappa$ OR and SmBiT- $\kappa$ OR at fixed plasmid ratios were treated with increasing concentrations of M $\beta$ CD prior to NanoBiT measurements. Cholesterol depletion resulted in a significant and concentration-dependent reduction in NanoBiT luminescence for WT  $\kappa$ OR (**Fig. 3h**), indicating a decreased population of  $\kappa$ OR dimers upon cholesterol removal.

To determine whether this effect reflects specific cholesterol-receptor interactions rather than a nonspecific disruption of membrane organization, we next examined  $\kappa$ OR mutants in which residues contacting cholesterol in the cryo-EM structure were substituted with alanine (**Fig. 3i**). Notably, for these cholesterol-interaction-deficient mutants (L79<sup>1.52</sup>A, F82<sup>1.55</sup>A, V278<sup>6.39</sup>A, L325<sup>7.48</sup>A, L328<sup>7.51</sup>A, L333<sup>7.46</sup>A), M $\beta$ CD treatment no longer produced a significant reduction in NanoBiT signal (**Fig. 3j**), indicating that the sensitivity of  $\kappa$ OR dimerization to cholesterol depletion depends on defined receptor-cholesterol contacts. Together, these results provide direct functional evidence that cholesterol molecules observed at the dimer interface in the cryo-EM

structure play a stabilizing role in  $\kappa$ OR dimer formation, rather than serving as passive membrane components.

### **$\kappa$ OR dimerization enhances G protein signal**

To characterize the dimer interface, we employed cysteine cross-linking experiments, a methodology previously utilized to analyze dimer interfaces in  $\beta_1$ AR and platelet-activating factor receptor (PAFR)<sup>43,46</sup>. Compared to  $\kappa$ OR WT, cysteine mutations in TM1 (V60<sup>1.33</sup>C, T63<sup>1.63</sup>C, and A64<sup>1.37</sup>C) resulted in a significant increase in the  $\kappa$ OR dimer ratio in the presence of CuP, consistent with our structural observations. Engineering the  $\kappa$ OR double mutants incorporating C315<sup>7.38</sup>A, which eliminates potential confounding effects of CuP, further increased the proportion of  $\kappa$ OR dimer formation (**Fig. 4a**). Notably, C315<sup>7.38</sup> is located on a different face of the receptor, approximately 90° removed from the TM1-Helix 8 dimer interface, and therefore does not directly contribute to protomer-protomer contacts. Surface expression levels and SalA binding affinities (pK<sub>i</sub> values) were comparable between all cysteine mutants and WT  $\kappa$ OR, indicating that the introduced mutations and receptor dimerization did not alter ligand affinity (**Fig. 4b-c**). Then in the presence of CuP treatment, which facilitate dimer formation, these  $\kappa$ OR mutants showed higher G<sub>i1</sub> signaling potency and efficacy upon SalA stimulation compared with WT and C315<sup>7.38</sup>A control  $\kappa$ OR (**Fig. 4d-e**), suggesting a functional relationship between receptor dimerization and enhanced G protein signaling, which was also found in PAFR dimer<sup>46</sup>.

We further investigated how signaling integrated within  $\kappa$ OR dimer. We used a luciferase complementation assay combined with BRET biosensor to specifically measure G protein recruitment to the  $\kappa$ OR dimer (**Fig. 4f**). In this experiment,  $\kappa$ OR was labeled with LgBiT and HiBiT, respectively, creating a linked configuration that facilitates the formation of a functional Nluc molecule when the two protomers ( $\kappa$ OR-LgBiT and  $\kappa$ OR-HiBiT) are brought together. This configuration allows for the detection of BRET signaling upon the recruitment of Venus-tagged miniG protein to the  $\kappa$ OR dimer labeled with complementary Nluc tags (**Fig. 4f**). Our results

revealed a significant reduction in G protein recruitment when one of the protomers was mutated at R156<sup>3,50</sup>A (impairing G protein coupling), by approximately 55% compared to WT dimers (**Fig. 4g**). These results indicate that maximal activation of the  $\kappa$ OR dimer depends on two functional protomers, with each protomer contributing independently to G protein recruitment. It is consistent with our structural analysis that the SalA-bound  $\kappa$ OR dimer could simultaneously engage two G proteins (**Fig. 2a**), and is different from previously characterized GPCR dimers, including, Class D Ste2 dimer<sup>28,29</sup>, Class C GPCRs and APJ dimers<sup>31,33,34,47</sup>, typically couple with only a G protein. Collectively, our results demonstrate that cysteine cross-linking enhances  $\kappa$ OR dimerization, consequently potentiating G<sub>i</sub> protein activation. The moderate effects observed with interface mutations suggest the dynamic nature and compensatory mechanisms inherent to lipid-mediated membrane protein dimerization.

## Discussion

The recognition that receptor dimerization occurs across diverse GPCR families and influences signaling pathways and pharmacological properties has fundamentally transformed our understanding of GPCR signaling paradigms<sup>18,20,48,49,50,51</sup>. This widespread phenomenon presents promising therapeutic opportunities through targeting multimeric receptor complexes. For ORs, persistent side effects continue to limit clinical utility, making therapeutic strategies directed at OR homo/heterodimers particularly attractive as complementary approaches alongside the development of low-efficacy/G<sub>i</sub>-biased ligands, allosteric modulators, and peptide therapeutics. However, the molecular mechanisms and functional consequences of dimerization remain poorly characterized for most class A GPCRs. Our study provides direct structural characterization for  $\kappa$ OR dimerization through cryo-EM analysis of SalA-bound  $\kappa$ OR dimers, revealing a 2:2 configuration with two G<sub>i</sub> proteins. In addition, we demonstrate its functional role in G protein signaling enhancement.

Our structural analysis identifies a lipid-mediated dimer interface between the two  $\kappa$ OR protomers

---

at TM1-Helix 8. Multiple fatty acids and cholesterol molecules occupy the interstitial space between protomers, suggesting that membrane lipids contribute to stabilizing the assembly by bridging hydrophobic residues such as V75<sup>1.48</sup>, F341<sup>8.54</sup> and F346<sup>8.59</sup>. Quantitative analysis shows that the buried surface area of this interface is 469 Å<sup>2</sup>, markedly smaller than those of previously characterized TM1-TM1 GPCR dimers, such as rhodopsin dimer<sup>42</sup> and β<sub>1</sub>AR dimer<sup>42</sup>. This relatively small contact area, together with lipid-mediated stabilization, represents a distinct and potentially generalizable mechanism for GPCR dimerization.

κOR dimerization enables simultaneous coupling of two G proteins in a 2:2 stoichiometry, in contrast with class C GPCRs and the well-documented GPR3 and apelin receptor dimers<sup>30, 31, 32, 33</sup>, where a single G protein couples per dimer and underscores the diversity of dimerization mechanisms across GPCR classes. This configuration provides a molecular basis for the enhanced κOR signaling potency and efficacy we observed, as both protomers contribute to G protein recruitment. The enhanced G<sub>i</sub> signaling observed in dimers, corroborated by our previous findings with PAFR<sup>46</sup>, suggests that dimerization amplifies receptor signaling through cooperative G protein coupling. BRET experiments demonstrate that mutations impairing G protein coupling in either protomer reduce overall signaling efficiency, indicating that κOR dimers may rely on contributions from both protomers to achieve optimal signaling output.

Structural analysis demonstrates that SalA recognition mechanisms are conserved between monomeric and dimeric receptor states. SalA establishes extensive interactions within the κOR orthosteric binding pocket, accounting for its potent and selective binding properties. The selectivity profile is primarily driven by critical interactions with Y312<sup>7.35</sup>, a residue that confers subtype specificity across OR families. Comparative structural analysis with μOR, δOR, and NOPR reveals that the distinctive van der Waals and polar interactions between Y312<sup>7.35</sup> and SalA's diterpenoid core underlie κOR's preferential activation. These structural insights establish SalA as a valuable pharmacophore template for rational design of κOR-selective therapeutic agents.

In conclusion, this study advances our understanding of  $\kappa$ OR biology by elucidating the structural basis of  $\kappa$ OR dimerization and its functional implications in opioid pharmacology. The integration of cryo-EM structural data with biochemical and mutagenesis analyses illuminates the mechanisms underlying  $\kappa$ OR dimer formation and its impact on receptor signaling. These findings improve our understanding of  $\kappa$ OR dimerization and its significance on receptor signaling, providing a structural framework that may guide future studies exploring  $\kappa$ OR dimer-targeted strategies a potential avenue for developing superior analgesics for pain and related disorders.

## Methods

### Constructs

To determine the structure of SalA-bound  $\kappa$ OR- $G_i$  complex, the sequence encoding the WT  $\kappa$ OR (3-380) was constructed into the pFastBac vector (ThermoFisher) with an N-terminal FLAG tag and a C-terminal His8 tag for two-step purification. The prolactin precursor sequence was fused to the very N-terminus as a signaling peptide to facilitate expression and  $\kappa$ OR anchoring to the cell membrane. Four dominant-negative mutations, G203A, A326S, S47N and E245A, were introduced into the human  $G_{\alpha i1}$  ( $G_{\alpha i1\_4M}$ ) by site-directed mutagenesis to decrease nucleotide binding affinity and stabilize the receptor- $G_i$  complex<sup>1</sup>. All the three components of  $G_{i1}$  heterotrimer, human  $G_{\alpha i1\_4M}$ , rat  $G_{\beta 1}$  and bovine  $G_{\gamma 2}$ , were constructed into the pFastBac vector (ThermoFisher), respectively.

### Expression and purification of the $\kappa$ OR- $G_i$ signaling complex

The purification of the single chain antibody scFv16 was completed in advance. The scFv16 sequence was fused with an N-terminal GP67 signaling peptide and a C-terminal TEV cleavage site-His8, and then cloned into the pFastBac vector (Thermo Fisher). The scFv16 stocks were prepared as previously described<sup>2,3</sup>.

For the  $\kappa$ OR-G<sub>i</sub> complex,  $\kappa$ OR, G<sub>ai1\_4M</sub>, G<sub>β1</sub> and G<sub>γ2</sub> were co-expressed in Sf9 insect cells using the Bac-to-Bac baculovirus expression system (ThermoFisher). The cells were cultured in ESF 921 serum-free medium (Expression Systems) to a density of  $4 \times 10^6$  cells/mL and then infected with the four types of baculoviruses expressing  $\kappa$ OR, G<sub>ai1\_4M</sub>, G<sub>β1</sub> and G<sub>γ2</sub> at a ratio of 1:1:1:1. After 48 hours of infection, the cells were collected by centrifugation at  $631 \times g$  for 20 minutes and the cell pellets were stored at  $-80^\circ\text{C}$  for further purification.

For the purification of  $\kappa$ OR-G<sub>i</sub> complex, cell pellets from 1L culture were thawed at room temperature and resuspended in 20 mM HEPES pH 7.2, 50 mM NaCl, 10 mM KCl, 5 mM MgCl<sub>2</sub>, 0.3 mM TCEP, protease inhibitor cocktail (Bimake, 1mL/100mL suspension). The suspension was treated with French Press and centrifuged at  $100,000 \times g$  for 30 min at  $4^\circ\text{C}$ . The cell precipitates were then collected and resuspended in a buffer containing 20 mM HEPES pH 7.2, 75 mM NaCl, 5 mM CaCl<sub>2</sub>, 5 mM MgCl<sub>2</sub>, 5% glycerol, 0.3 mM TCEP, protease inhibitor cocktail (Bimake, 1 mL/100 mL suspension). The  $\kappa$ OR-G<sub>i</sub> complex was formed on the membrane by the addition of 10  $\mu\text{M}$  Sal A and incubating for half an hour at room temperature. The suspension was treated with 25 mU/mL apyrase to digest the nucleotides. After incubating for an additional hour at room temperature, the complex was extracted from the membrane using 0.5% (w/v) lauryl maltose neopentylglycol (LMNG, Anatrace) and 0.1% (w/v) cholesteryl hemisuccinate TRIS salt (CHS, Anatrace) for 3 hours at  $4^\circ\text{C}$ . The solubilized fractions were isolated by centrifugation at  $100,000 \times g$  for 45 min and then incubated overnight at  $4^\circ\text{C}$  with pre-equilibrated Nickel-NTA resin. After batch binding, the nickel resin with immobilized protein complex was manually loaded onto a gravity column. The resin was first washed with 20 column volumes of a buffer consisting of 20 mM HEPES, pH 7.2, 100 mM NaCl, 40 mM imidazole, 0.3 mM TCEP, 0.05% LMNG (w/v), 0.01% CHS (w/v), and 10  $\mu\text{M}$  SalA, and then eluted using the same buffer containing 300 mM imidazole.

The eluted protein was further incubated with 2.5 mg scFv16 by batch binding with 2 mL FLAG resin (Smart-Lifesciences) for 2 hours at  $4^\circ\text{C}$ . The FLAG resin with protein complex was then

washed by 10 column volumes of detergent buffer containing 20 mM HEPES, pH 7.2, 100 mM NaCl, 0.3 mM TCEP, 0.0075% LMNG (w/v), 0.0025% GDN, 0.002% CHS (w/v), 10  $\mu$ M SalA. Subsequently, the material bound to FLAG resin was then eluted with the same detergent buffer containing 200 $\mu$ g/ $\mu$ L FLAG peptide. The complex was concentrated to 0.5ml by using an Ultra Centrifugal Filter (Millipore, Sigma, 100 kDa molecular weight cutoff) and loaded onto a Superdex 200, 10/300 GL increase column (GE Healthcare) pre-equilibrated with a buffer containing 20 mM HEPES, pH 7.2, 100 mM NaCl, 0.00075% LMNG (w/v), 0.00025% GDN, 0.0002% CHS (w/v), 0.3 mM TCEP, and 10  $\mu$ M SalA. Fractions from the main peak of the protein complex was separately collected and concentrated for electron microscopy experiments.

#### **Cryo-EM grid preparation and data collection**

For cryo-EM grid preparation, 3.0  $\mu$ L of each concentrated sample corresponding to two peaks was applied onto glow-discharged EM grids (Quantifoil R1.2/1.3 holey carbon films, 300 mesh Au) within a Vitrobot chamber (FEI Vitrobot Mark IV). Vitrification was conducted at 100% humidity and 4 °C, with the sample blotted for 3 s prior to plunge-freezing into liquid ethane. The cryo-EM grids prepared in this manner were subsequently stored in liquid nitrogen for screening and subsequent data collection purposes.

For the SalA- $\kappa$ OR-G<sub>i</sub>-scFv16 monomer, cryo-EM movie stacks were acquired automatically on an FEI Titan Krios microscope operating at 300 kV within the Advanced Center for Electron Microscopy at the Shanghai Institute of Materia Medica, Chinese Academy of Sciences (Shanghai, China). The microscope was outfitted with a Gatan Quantum energy filter. Movie stacks were collected using a Gatan K3 direct electron detector, operating at a nominal magnification of 105,000 $\times$  in super-resolution counting mode with a pixel size of 0.824 Å. The energy filter utilized a slit width of 20 eV. Each movie stack comprised 36 frames dose-fractionated at 1.39 electrons per frame, acquired with a defocus ranging from -0.8 to -2.0  $\mu$ m. The total exposure time per stack was 2.35 s. A total of 6,632 movie stacks were recorded for the SalA- $\kappa$ OR-G<sub>i</sub>-scFv16 monomer,

---

employing EPU software for data collection with one exposure per hole on the grid squares. During 3D classification in the data processing, a cluster of dimers was reconstructed using 8,167 particles. Consequently, 21,486 movies were added for further processing of the dimers. The same conditions were applied across this dataset collection to combine these movies.

### **Image processing and 3D reconstruction**

All dose-fractionated images were motion-corrected and dose-weighted using MotionCorr2 software, and their contrast transfer functions (CTF) were estimated with CTFFIND4.1 in RELION4.0. Micrographs with resolutions worse than 4.0 Å and those containing grid carbon areas were excluded from further analysis. For the monomer complex, 5,732 movies were retained for subsequent data processing. The previously solved map of dynorphin A<sub>1-13</sub>-κOR-G<sub>i</sub>-scFv16 (PDB: 8F7W), low-pass filtered to 40 Å, served as a template for auto-picking, resulting in 4,440,103 particles for interactive 2D and 3D classifications. Following multiple rounds of 3D classification, 204,668 high-quality particles were selected. These particles underwent 3D refinement, CTF refinement, Bayesian polishing, and post-processing in DeepEMhancer, yielding a density map with a reported global resolution of 3.3 Å at a Fourier shell correlation (FSC) of 0.143. During the data processing, a minor population of SalA-κOR-G<sub>i</sub> dimers was identified through 3D classification. Using this low-resolution dimer as a template for particle picking yielded only a small fraction of particles. Subsequently, additional data collection was conducted as mentioned above, merging two datasets. Using dimer as template, 22,715,217 particles were picked. These particles were randomly split into eight subsets, each subset was combined with the dimer-template particle set using RELION's *join star file* operation and then subjected to independent 3D classification, after which redundant particles were removed. The selected particles were combined and subjected to further rounds of 3D classification, resulting in the selection of 41,577 particles for the final map generation. For the dimeric κOR-G<sub>i</sub> structure, C2 symmetry was applied during 3D classification and refinement, which improved both global resolution and the clarity of the TM1-Helix 8 interface. The final refinement outputs were then

used to generate two complementary map representations from the same refined particle set: (i) a conventionally post-processed map generated in RELION (9UXX) and (ii) a DeepEMhancer-processed map (9UXU). Both maps reached an overall resolution of 3.6 Å (FSC = 0.143). The primary difference between these two map representations is the appearance of non-protein densities at the dimer interface, with the conventionally post-processed map more consistently preserving sterol-/lipid-like features at the interface, whereas DeepEMhancer preferentially enhances continuous protein features.

### **Model building, structure refinement, and figure preparation**

The previously published structure of the  $\kappa$ OR-G<sub>i</sub> complex (PDB: 8F7W) served as the starting model for both the model building and refinement of the SalA- $\kappa$ OR-G<sub>i</sub>-scFv16 monomer and dimer. Initially, structural models were rigidly docked into the cryo-EM density maps using UCSF Chimera<sup>52</sup>, followed by manual rebuilding and adjustment in COOT<sup>53</sup>. Real-space and Rosetta refinements were conducted using Phenix<sup>54</sup>. The SalA ligand was generated using Phenix's elbow module from a SMILES string input. Model quality was assessed using MolProbity<sup>55</sup>. Structural representations were prepared using Chimera and PyMOL (<https://pymol.org/2/>). Detailed refinement statistics can be found in **Supplementary Table 1**. Maximum distance cutoffs for polar hydrogen-bond interactions and hydrophobic interactions were set at 3.5 Å and 4.5 Å, respectively.

### **GloSensor cAMP assay**

The GloSensor cAMP assay (Promega)<sup>4</sup> was utilized to detect dynamic changes in intracellular cAMP levels induced by ORs. Briefly, sequences of ORs, fused with an HA signal peptide and FLAG tag, were cloned into a pcDNA3.0 vector for expression in the HEK293T system. Before transfection, HEK293T cells were plated onto a 6-well plate (3 mL/well) at a density of  $2 \times 10^5$  cells/mL. After 16 hours, cells were transfected with 1.5  $\mu$ g receptor DNA and 1  $\mu$ g GloSensor-22F (Promega) DNA. After 24 hours, transfected cells were resuspended in CO<sub>2</sub>-independent media and transferred to a 384-well plate at a density of  $6 \times 10^5$  cells/mL in a volume of 20  $\mu$ L per

well. After a short centrifugation, 10  $\mu$ L CO<sub>2</sub>-independent media containing 2% GloSensor cAMP Reagent (Promega) was added and incubated at 37 °C for 1 hour. Subsequently, 10  $\mu$ L SalA (4 $\times$ ) containing 4  $\mu$ M forskolin were added and incubated for 10 minutes at room temperature. After incubation, luminescence signals were tested by EnVision multi-plate reader according to the manufacturer's instructions. All data were analyzed using Prism 9 (GraphPad) and presented as mean  $\pm$  S.E.M. from at least three independent experiments, each performed in technical duplicates or triplicates. Non-linear curve fit was performed using a three-parameter logistic equation [log (agonist vs response)].

### **BiFC assay**

HEK293 cells (ATCC, CRL-1573, lot: 3449904) were transfected with  $\kappa$ OR with complementary components of Venus fluorescent protein (VN or VC) fused in the C-terminus for BiFC assay as described previously<sup>56</sup>. Twenty-four hours after transfection, the growth media and transfection reagent were replaced with PBS, and images were acquired using an Olympus FV3000 Laser Scanning Confocal Microscope (60  $\times$  objective, Olympus, Tokyo, Japan) equipped with appropriate fluorescence and filters (GFP, 488/519 nm). The images were digitized and saved in TIFF format. respectively, more than five microscopic fields were randomly chosen for analysis. Images were processed and fluorescence was quantified with Fiji (ImageJ) and the MorphoLibJ plugin were used to determine the fluorescence intensity of each cell membrane<sup>57</sup>.

### **Cell surface quantification by ELISA**

ELISA was performed for detection of the HA-tagged  $\kappa$ OR WT at the cell surface. 24 h after transfection, the HEK293 cells were fixed with 4% paraformaldehyde, blocked with 10% FBS. HA-tagged  $\kappa$ OR were detected with a monoclonal rat anti-HA antibody (with horseradish peroxidase) 3F10 (Roche) at 0.5  $\mu$ g/mL. FLAG-tagged constructs were detected with the mouse monoclonal anti-FLAG antibody (with horseradish peroxidase) M2 (Sigma, St. Louis, MO) at 1.0

$\mu\text{g/mL}$ . Bound antibodies coupled to horseradish peroxidase were detected by chemoluminescence using SuperSignal substrate (Pierce) and read using the Tecan infinite 200Pro (Swiss).

### **NanoBiT assay**

The NanoBiT Protein-Protein interaction system (Promega) was utilized to assess the interaction between LgBiT- $\kappa\text{OR}$  and SmBiT- $\kappa\text{OR}$ . Briefly, HEK293T cells were co-transfected with plasmids encoding LgBiT- $\kappa\text{OR}$  mutants and SmBiT- $\kappa\text{OR}$  mutants at the ratio of 1:1. After 24 hours, cells were harvested and resuspended in PBS buffer to a density of  $6 \times 10^5$  cells/mL. Subsequently, 10  $\mu\text{L}$  of the cell suspension was transferred into a 384-well plate, followed by the addition of 10  $\mu\text{L}$  SalA (3 $\times$ ) and 10  $\mu\text{L}$  coelenterazine 400a (Yeasen) with a final concentration of 50  $\mu\text{M}$ . After a 10-minute incubation at room temperature, luminescence was measured with an EnVision multiplate reader (PerkinElmer).

LgBiT and SmBiT were also fused to the C-terminal of  $\kappa\text{OR}$  (as  $\kappa\text{OR}$ -LgBiT and  $\kappa\text{OR}$ -SmBiT) to confirm the basal and agonist effect on dimerization. Briefly, HEK293 cells were co-transfected with plasmids encoding  $\kappa\text{OR}$ -LgBiT and  $\kappa\text{OR}$ -SmBiT at the ratio of 1:1 and seeded in 96-well plate. After 24 hours, cells were starved in PBS for 1h. Then the indicated agonist and 10  $\mu\text{M}$  furimazine were added to cells. The signals emitted by the Nluc (460-500 nm band-pass filter, Em 480) were recorded immediately using PHERAstar FS (BMG Labtech, USA). The luminescence at 10 minutes was used for data analysis.

### **Cross-linking and fluorescent-labeled blot experiments**

HEK293 cells were transfected with FLAG-Halo- $\kappa\text{OR}$  WT or indicated mutants by lipofectamine 2000 and plated in 12-well plates for 36 h. Then cells were labeled with 100 nM Halo-660 non-cell permeant in culture medium at 37°C for 2 h. Cells were incubated with PBS at 37 °C for 30 min. Afterwards, cross-link buffer (1.5 mM Cu(II)-(o-phenanthroline), 1 mM CaCl<sub>2</sub>, 5 mM Mg<sup>2+</sup>,

16.7 mM Tris HCl, pH 8.0 and 100 mM NaCl) was added at 37 °C for 20 min. After incubation with 10 mM N-ethylmaleimide at 4 °C for 15 min to stop the cross-linking reaction, cells were lysed with lysis buffer (containing 50 mM Tris pH 7.4, 150 mM NaCl, 1% NP-40 and 0.5% sodium deoxycholate) at 4 °C for 1.5 h. After centrifugation at  $12,000 \times g$  for 30 min at 4 °C, supernatants were mixed with loading buffer at 37 °C for 10 min. In reducing conditions, samples were treated without DTT in loading buffer for 10 min before loading the samples. Equal amounts of proteins were resolved by 59:1 acrylamide:bisacrylamide and 6% SDS-PAGE. Proteins were transferred to nitrocellulose membranes (Millipore). Membrane was imaged on an Odyssey CLx imager (LI-COR Bioscience, Lincoln, NE, USA) at 700 nm.

### **Bioluminescence resonance energy transfer (BRET) assay**

For the detection of the  $G_{i1}$  protein activation, HEK293 cells were transfected with WT or mutant  $\kappa$ OR,  $G_{ai1}$ -Nluc,  $G_{\beta 1}$ , Venus- $G_{\gamma 2}$  and EAAC1. Lipofectamine 2000 was used for the cDNA transfection into HEK293 cells. After 24 h transfection, cells were incubated with PBS at 37°C for 30 min. Afterwards, cross-link buffer (1.5 mM Cu(II)-(o-phenanthroline), 1 mM  $CaCl_2$ , 5 mM  $Mg^{2+}$ , 16.7 mM Tris HCl, pH 8.0 and 100 mM NaCl) was added at 37 °C for 20 min. Cells were washed three times with PBS, before performing BRET1 measurement. For miniG protein recruitment, BRET assays were used as previously documented<sup>46,58</sup>. HEK293 cells were transfected with Venus-miniG $i1$  together with  $\kappa$ OR-LgBiT and  $\kappa$ OR-HiBiT WT or mutant to form complementary  $\kappa$ OR dimer. After 24 h transfection, cells were washed and starved in PBS at 37 °C for 1 h, before performing BRET1 measurement. BRET1 measurements were performed using PHERAstar FS (BMG Labtech, USA). The signals emitted by the donor (460-500 nm band-pass filter, Em 480) and the acceptor entity (510-550 nm band-pass filter, Em 530) were recorded after the addition of 10  $\mu$ M furimazine. The BRET signal was determined by calculating the ratio between the emission of acceptor and donor (Em 530 / Em 480). The basal BRET ratio (BRET<sub>basal</sub>) of cells was recorded before the stimulation with drugs or buffer. The change in BRET ratio (net

BRET) was obtained by subtracting the BRET ratio between agonist treatment and the basal BRET to get a positive value.

### **Radioligand binding assay**

Binding assays were conducted using crude membrane preparations made from HEK293T cells transiently transfected with  $\kappa$ OR. The radioligand [ $^3$ H]U-69,593 was used to label  $\kappa$ OR at a final concentration around  $K_d$ . Briefly, 50  $\mu$ L of membrane suspension was co-incubated with 50  $\mu$ L of  $2.5 \times$  [ $^3$ H]U-69,593 and 25  $\mu$ L of  $5 \times$  test compound in standard assay buffer (50 mM Tris-HCl, pH 7.4, with 10 mM MgCl<sub>2</sub> and 0.1 mM EDTA), supplemented with 1 mg/mL fatty-acid free bovine serum albumin. After incubation for 60 minutes at room temperature, membranes were collected by vacuum filtration onto PEI-coated GF/C filter-bottom 96-well plates and washed three times under vacuum with cold harvesting buffer (50 mM Tris-HCl, pH 7.4). Non-specific binding was determined in the presence of 1  $\mu$ M dynorphin A or salvinorin A. Data were analyzed using GraphPad Prism.

### **Detection of surface expression**

$\kappa$ OR mutants with an N-terminal FLAG tag were transiently expressed in HEK293T cells as described for the NanoBiT assay. After 24 hours, transfected cells cultured in 12-well plates were washed once with PBS and resuspended in PBS to achieve a density of  $5-6 \times 10^5$  cells/mL. Cells were then incubated with anti-FLAG FITC-conjugated antibody (Sigma-Aldrich) diluted 1:100 in blocking buffer (PBS supplemented with 5% BSA) at 4 °C for 15 min. Cell surface expression of  $\kappa$ OR WT and mutants were analyzed using a Guava easyCyte flow cytometer (Luminex). For each sample, 5000 cellular events were collected and data were normalized to WT. The gating strategy and the method used for expression calculation are shown in Supplementary Fig. 10.

### **Cholesterol depletion assay**

Acute depletion of plasma membrane cholesterol was performed using methyl- $\beta$ -cyclodextrin (MCD). Briefly, HEK293T cells were co-transfected with plasmids encoding LgBiT- $\kappa$ OR and SmBiT- $\kappa$ OR at a 1:1 ratio. After 24 hours, cells were harvested and resuspended in PBS to a density of  $4 \times 10^6$  cells/mL. 30mM MCD stock solution was freshly prepared in PBS and diluted to various working concentrations prior to use. Cells were then incubated with equal volumes of MCD solutions at 37 °C for 20 minutes to acutely deplete membrane cholesterol. After depletion, cells were washed with PBS to remove residual MCD and resuspended in PBS. The cell suspension was then plated onto 384-well plates in a volume of 20  $\mu$ L per well, followed by the addition of 10  $\mu$ L coelenterazine 400a (Yeasen) with a final concentration of 50  $\mu$ M. Luminescence signal was measured using an EnVision multiplate reader (PerkinElmer).

### **Mass photometry analysis**

Mass photometry measurements were performed using a Refeyn TwoMP mass photometer. Briefly, 10  $\mu$ L of the filtered measurement buffer was added to a cleaned coverslip to set the focus, followed by the addition of 10  $\mu$ L diluted  $\kappa$ OR sample, the final concentration is 10 nM. Movies were recorded for 1 min, and the molecular mass of the sample was determined by linear calibration against a standardized protein mixture, in this case, IgG was used as standard. All data were analyzed using DiscoverMP.

### **Data Availability**

The cryo-EM density maps have been deposited in the Electron Microscopy Data Bank under accession numbers EMD-64564 [<https://www.ebi.ac.uk/emdb/EMD-64564>] (monomeric  $\kappa$ OR-G<sub>i</sub>-scFv16 complex bound to SalA) and EMD-64604 [<https://www.ebi.ac.uk/emdb/EMD-64604>], EMD-64602 [<https://www.ebi.ac.uk/emdb/EMD-64602>] (dimeric  $\kappa$ OR-G<sub>i</sub>-scFv16 complex bound

to SalaA, post-processing and DeepEMhancer map). The corresponding atomic coordinates have been deposited in the Worldwide Protein Data Bank (wwPDB) under accession numbers 9UWV [<http://doi.org/10.2210/pdb9UWV/pdb>], 9UXX [<http://doi.org/10.2210/pdb9UXX/pdb>], and 9UXU [<http://doi.org/10.2210/pdb9UXU/pdb>], respectively. All other data supporting the findings of this study are available in the main text and supplementary figures and tables. Source data are provided with this paper.

## References

1. Friedman A, Nabong L. Opioids: Pharmacology, Physiology, and Clinical Implications in Pain Medicine. *Physical medicine and rehabilitation clinics of North America* **31**, 289-303 (2020).
2. Spencer MR, Miniño AM, Warner M. Drug Overdose Deaths in the United States, 2001-2021. *NCHS data brief*, 1-8 (2022).
3. Bruijnzeel AW. kappa-Opioid receptor signaling and brain reward function. *Brain Res Rev* **62**, 127-146 (2009).
4. Shippenberg TS, Chefer VI, Zapata A, Heidbreder CA. Modulation of the behavioral and neurochemical effects of psychostimulants by kappa-opioid receptor systems. *Ann N Y Acad Sci* **937**, 50-73 (2001).
5. Dalefield ML, Scouller B, Bibi R, Kivell BM. The Kappa Opioid Receptor: A Promising Therapeutic Target for Multiple Pathologies. *Front Pharmacol* **13**, 837671 (2022).
6. Machelska H, Celik MO. Advances in Achieving Opioid Analgesia Without Side Effects. *Front Pharmacol* **9**, 1388 (2018).
7. Simonin F, *et al.* kappa-Opioid receptor in humans: cDNA and genomic cloning, chromosomal assignment, functional expression, pharmacology, and expression pattern in the central nervous system. **92**, 7006-7010 (1995).
8. Kaski SW, White AN, Gross JD, Siderovski DP. Potential for Kappa-Opioid Receptor Agonists to Engineer Nonaddictive Analgesics: A Narrative Review. **132**, 406-419 (2021).
9. Wu H, *et al.* Structure of the human kappa-opioid receptor in complex with JD1c. *Nature* **485**, 327-332 (2012).

10. Che T, *et al.* Structure of the Nanobody-Stabilized Active State of the Kappa Opioid Receptor. *Cell* **172**, 55-67 e15 (2018).
11. Han J, *et al.* Ligand and G-protein selectivity in the kappa-opioid receptor. *Nature* **617**, 417-425 (2023).
12. El Daibani A, *et al.* Molecular mechanism of biased signaling at the kappa opioid receptor. *Nat Commun* **14**, 1338 (2023).
13. Wang Y, *et al.* Structures of the entire human opioid receptor family. *Cell* **186**, 413-427 e417 (2023).
14. Suno-Ikeda C, *et al.* Structural and dynamic insights into the biased signaling mechanism of the human kappa opioid receptor. *Nature communications* **16**, 9392 (2025).
15. Guerrero M, *et al.* Design and Synthesis of a Novel and Selective Kappa Opioid Receptor (KOR) Antagonist (BTRX-335140). *J Med Chem* **62**, 1761-1780 (2019).
16. Zheng Z, *et al.* Structure-Based Discovery of New Antagonist and Biased Agonist Chemotypes for the Kappa Opioid Receptor. *J Med Chem* **60**, 3070-3081 (2017).
17. Wala K, Szepietowski JC. Difelikefalin in the Treatment of Chronic Kidney Disease-Associated Pruritus: A Systematic Review. *Pharmaceuticals* **15**, (2022).
18. Ferre S, *et al.* G protein-coupled receptor oligomerization revisited: functional and pharmacological perspectives. *Pharmacological reviews* **66**, 413-434 (2014).
19. Gomes I, Ayoub MA, Fujita W, Jaeger WC, Pflieger KD, Devi LA. G Protein-Coupled Receptor Heteromers. *Annual review of pharmacology and toxicology* **56**, 403-425 (2016).
20. Moreno E, *et al.* Pharmacological targeting of G protein-coupled receptor heteromers. *Pharmacol Res* **185**, 106476 (2022).
21. Cvejic S, Devi LA. Dimerization of the delta opioid receptor: implication for a role in receptor internalization. *J Biol Chem* **272**, 26959-26964 (1997).
22. Moller J, *et al.* Single-molecule analysis reveals agonist-specific dimer formation of micro-opioid receptors. *Nat Chem Biol* **16**, 946-954 (2020).
23. Jordan BA, Devi LA. G-protein-coupled receptor heterodimerization modulates receptor function. *Nature* **399**, 697-700 (1999).

- 
24. Wang D, Sun X, Bohn LM, Sadee W. Opioid receptor homo- and heterodimerization in living cells by quantitative bioluminescence resonance energy transfer. *Mol Pharmacol* **67**, 2173-2184 (2005).
  25. Zhou P, *et al.* Single-molecule methods for characterizing receptor dimers reveal metastable opioid receptor homodimers that induce functional modulation. *Nature Communications* **16**, 9858 (2025).
  26. Cechova K, Lan C, Macik M, Barthes NPF, Jung M, Ulbrich MH. Kappa but not delta or mu opioid receptors form homodimers at low membrane densities. *Cell Mol Life Sci* **78**, 7557-7568 (2021).
  27. Zhou P, *et al.* Single-molecule characterization of opioid receptor heterodimers reveals soluble  $\mu$ - $\delta$  dimer blocker peptide alleviates morphine tolerance. *Nature Communications* **16**, 9859 (2025).
  28. Velazhahan V, *et al.* Structure of the class D GPCR Ste2 dimer coupled to two G proteins. *Nature* **589**, 148-153 (2021).
  29. Velazhahan V, Ma N, Vaidehi N, Tate CG. Activation mechanism of the class D fungal GPCR dimer Ste2. *Nature* **603**, 743-748 (2022).
  30. Yue Y, *et al.* Structural insight into apelin receptor-G protein stoichiometry. *Nat Struct Mol Biol* **29**, 688-697 (2022).
  31. Yue Y, *et al.* Structural insights into the regulation of monomeric and dimeric apelin receptor. *Nature Communications* **16**, 310 (2025).
  32. Chang H, *et al.* Structural basis of oligomerization-modulated activation and autoinhibition of orphan receptor GPR3. *Cell Reports* **44**, 115478 (2025).
  33. Wang X, *et al.* Structural insights into dimerization and activation of the mGlu2–mGlu3 and mGlu2–mGlu4 heterodimers. *Cell Res* **33**, 762-774 (2023).
  34. Ma X, *et al.* Molecular insights into the activation mechanism of GPR156 in maintaining auditory function. *Nature Communications* **15**, 10601 (2024).
  35. Roth BL, *et al.* Salvinorin A: A potent naturally occurring nonnitrogenous  $\kappa$  opioid selective agonist. *Proceedings of the National Academy of Sciences* **99**, 11934-11939 (2002).
  36. Ballesteros JA, Weinstein H. Integrated methods for the construction of three-dimensional models and computational probing of structure-function relations in G protein-coupled receptors. *Methods in Neurosciences* **25**, 366-428 (1995).
  37. Xu P, *et al.* Structural genomics of the human dopamine receptor system. *Cell Res* **33**, 604-616 (2023).

- 
38. Liu H, *et al.* Recognition of methamphetamine and other amines by trace amine receptor TAAR1. *Nature* **624**, 663-671 (2023).
  39. Xu P, *et al.* Structural insights into the lipid and ligand regulation of serotonin receptors. *Nature* **592**, 469-473 (2021).
  40. Puls K, Wolber G. Solving an Old Puzzle: Elucidation and Evaluation of the Binding Mode of Salvinorin A at the Kappa Opioid Receptor. *Molecules* **28**, (2023).
  41. Wang Y, *et al.* Comparison of Pharmacological Activities of Three Distinct  $\kappa$  Ligands (Salvinorin A, TRK-820 and 3FLB) on  $\kappa$  Opioid Receptors in Vitro and Their Antipruritic and Antinociceptive Activities in Vivo. *The Journal of Pharmacology and Experimental Therapeutics* **312**, 220-230 (2005).
  42. Zhao DY, *et al.* Cryo-EM structure of the native rhodopsin dimer in nanodiscs. *J Biol Chem* **294**, 14215-14230 (2019).
  43. Huang J, Chen S, Zhang JJ, Huang XY. Crystal structure of oligomeric beta1-adrenergic G protein-coupled receptors in ligand-free basal state. *Nat Struct Mol Biol* **20**, 419-425 (2013).
  44. Leslie AGW, Warne T, Tate CG. Ligand occupancy in crystal structure of  $\beta$ 1-adrenergic G protein-coupled receptor. *Nat Struct Mol Biol* **22**, 941-942 (2015).
  45. Zhang H, *et al.* Dimerization and antidepressant recognition at noradrenaline transporter. *Nature* **630**, 247-254 (2024).
  46. Liu J, *et al.* Biased signaling due to oligomerization of the G protein-coupled platelet-activating factor receptor. *Nat Commun* **13**, 6365 (2022).
  47. Yue Y, *et al.* Structural insight into apelin receptor-G protein stoichiometry. *Nat Struct Mol Biol* **29**, 688-697 (2022).
  48. Faron-Gorecka A, *et al.* Understanding GPCR dimerization. *Methods Cell Biol* **149**, 155-178 (2019).
  49. Asher WB, *et al.* Single-molecule FRET imaging of GPCR dimers in living cells. *Nature methods* **18**, 397-405 (2021).
  50. George SR, O'Dowd BF, Lee SP. G-protein-coupled receptor oligomerization and its potential for drug discovery. *Nature reviews Drug discovery* **1**, 808-820 (2002).

- 
51. Dziedzicka-Wasylewska M, Polit A, Blasiak E, Faron-Gorecka A. G Protein-Coupled Receptor Dimerization-What Next? *International journal of molecular sciences* **25**, (2024).
  52. Pettersen EF, *et al.* UCSF Chimera--a visualization system for exploratory research and analysis. *J Comput Chem* **25**, 1605-1612 (2004).
  53. Emsley P, Cowtan K. Coot: model-building tools for molecular graphics. *Acta Crystallogr D Biol Crystallogr* **60**, 2126-2132 (2004).
  54. Adams PD, *et al.* PHENIX: a comprehensive Python-based system for macromolecular structure solution. *Acta Crystallogr D Biol Crystallogr* **66**, 213-221 (2010).
  55. Chen VB, *et al.* MolProbity: all-atom structure validation for macromolecular crystallography. *Acta Crystallogr D Biol Crystallogr* **66**, 12-21 (2010).
  56. Shyu YJ, Han L, Xuehong D, and Hu C-D. Identification of New Fluorescent Protein Fragments for Bimolecular Fluorescence Complementation Analysis Under Physiological Conditions. *BioTechniques* **40**, 61-66 (2006).
  57. Legland D, Arganda-Carreras I, Andrey P. MorphoLibJ: integrated library and plugins for mathematical morphology with ImageJ. *Bioinformatics* **32**, 3532-3534 (2016).
  58. Xu C, *et al.* Specific pharmacological and G(i/o) protein responses of some native GPCRs in neurons. *Nat Commun* **15**, 1990 (2024).

## Acknowledgements

The cryo-EM data of this study were collected at the Advanced Center for Electron Microscopy, Shanghai Institute of Materia Medica (SIMM). We thank all the staff at the center for their assistance in cryo-EM data collection. We also thank Shanghai Frontiers Science Center of Cellular Homeostasis and Human Diseases of Shanghai Jiao Tong University, School of Medicine for the technical support.

## Funding

This work was partially supported by grants from the National Natural Science Foundation of China (32400998 to Y.W., 32401002 to Y.W.Z., 32130022 and 82121005 to H.E.X., 32421003 to J.L.); the National Key R&D Program of China (2022YFA1302900 to H.E.X.; 2024YFA1307504 to Y.W.Z.); Strategic Priority Research Program of the Chinese Academy of Sciences Grant (No. XDB0830000, XDA0530000, XDB37030103 to H.E.X.); Shanghai Municipal Science and Technology Major Project (2019SHZDZX02 to H.E.X.); the Shanghai Municipal Science and Technology Major Project (H.E.X.); the Young Elite Scientists Sponsorship Program by CAST (2023QNRC001 to Y.W.Z.); the Natural Science Foundation of Shanghai, China (23ZR1475300 to Y.W.Z.); the Sailing Program of Shanghai Venus Project (23YF1456700 to Y.W.Z.); the “Shanghai Jiao Tong University 2030” Project-Category C (WH510363003/017 to Y.W.Z.); the Innovative Research Team of High-Level Local Universities in Shanghai (Y.W.Z.); the Support of SANOFI Scholarship Program (Y.W.Z.); and the HE Research Fellowship (HERF2025011 to Y.W.Z.)

## Author Contributions

Y.X.Z. performed the Glosensor assay, NanoBiT titration assay, cholesterol depletion assay, mass photometry, mutant expression assay and corresponding data preparation; C.J.X. guided Y.L. and X.L. for the BiFC, NanoBiT, crosslink and BRET experiments, and participated in the preparation of figures; Y.W. purified and prepared the protein samples of monomer and dimer of SalA-bound  $\kappa$ OR for cryo-EM grid making, performed cryo-EM structure determination and model building,

wrote the draft and prepared the figures; H.S. and J.L. assisted with dimer structure determination and model building; J.W., B.L.R. and X.P.H. performed the radioligand binding assay; M.Y.L. and Y.N.L. assisted in the cell-based functional data analysis and manuscript editing; K.W. collected the cryo-EM data. Y.W.Z., H.E.X and J.L. conceived and supervised the project, and wrote the manuscript with input from others.

### Competing Interests

H.E.X is a founder of Cascade Pharmaceuticals. All the other authors declare no competing interests.

### Figure legends

**Fig. 1 | ligand-independent  $\kappa$ OR dimerization in living cells.** **a**, Schematic representation of the BiFC assay. Venus fluorescent protein fragments (VN and VC) were fused to the C-terminus of  $\kappa$ OR tagged with either FLAG or HA at the N-terminus.  $\kappa$ OR dimerization brings VN and VC in close proximity, reconstituting Venus fluorescence. Co-expression of untagged  $\kappa$ OR competes for dimer formation and reduces BiFC signal. **b**, Representative BiFC images of HEK293 cells co-expressing FLAG- $\kappa$ OR-VN and FLAG- $\kappa$ OR-VC, in the absence or presence of untagged HA- $\kappa$ OR. Scale bar, 100  $\mu$ m. **c**, Quantification of membrane BiFC intensity. Fluorescence was measured from 26 and 36 cells respectively in two groups of cells with indicated transfection, from three independent experiments. Data are mean  $\pm$  S.E.M. analyzed using unpaired t test (two-tailed). ( $P < 0.0001$ ). \*\*\*\* $P < 0.0001$  vs. in the absence of untagged HA- $\kappa$ OR. Source data are provided as a Source Data file. **d**, Membrane expression of FLAG-tagged and HA-tagged  $\kappa$ OR measured by ELISA. Data are present as the fold of the luminescence intensity in transfected cells compared with mock cells. Data are presented as mean  $\pm$  S.E.M. from three independent biological replicates performed in technical triplicates. **e**, Effect of  $\kappa$ OR agonist treatment on dimerization efficiency measured by luciferase complementation (NanoBiT assay) between  $\kappa$ OR-LgBiT and  $\kappa$ OR-SmBiT fusion proteins. Cells co-expressing  $\kappa$ OR-LgBiT and  $\kappa$ OR-SmBiT were treated with indicated  $\kappa$ OR agonists (concentrations and duration). Data are presented as mean  $\pm$  S.E.M. from five independent biological replicates, each performed in technical triplicates, and analyzed using one-way ANOVA with a Dunnett's post-hoc multiple comparison test compared with PBS treatment to determine significance. ( $P=0.0093$ ,  $P=0.8652$ ,  $P=0.5522$ ,  $P=0.0248$ ,  $P=0.5574$  and  $P=0.2615$  from left to right). \*\* $P < 0.01$ , \* $P < 0.05$ ; ns, not significant  $P > 0.05$  vs. PBS. Source data are provided as a Source Data file.

**Fig. 2 | Structural basis and molecular recognition of Sala binding to  $\kappa$ OR.** **a-c**, Orthogonal views of the cryo-EM density maps and structural models of the Sala-bound  $\kappa$ OR-G<sub>i</sub> dimer complex in side view (**a**) and extracellular view (**b**), alongside the monomeric complex (**c**). Each

$\kappa$ OR protomer couples with a  $G_i$  protein in a parallel, mirror-symmetric arrangement, distinct from previously characterized GPCR dimers. Note: The cryo-EM data collection and refinement statistics is shown in Supplementary Table 1. **d**, Superposition of SalA, MP1104, and nalfurafine in the  $\kappa$ OR orthosteric binding pocket, revealing similar binding poses despite their chemical diversity. **e**, The 2D diagram depicting the interaction of SalA within the  $\kappa$ OR pocket. Pink represents residues with polar interactions, green represents residues with hydrophobic interactions, blue background indicates the exposure level of residues, and green arrows denote hydrogen bond interactions. **f and h**, The hydrophilic (**f**) and hydrophobic (**h**) interactions of SalA with  $\kappa$ OR. **g and i**, Concentration-response curves for the activation of mutated residues which contact with SalA. Data shown are mean  $\pm$  S.E.M. from at least three independent experiments ( $n=4$  for WT and  $n=3$  for mutants) performed in technical triplicate. Note: The numerical data with statistics is shown in Supplementary Table 2. Source data are provided as a Source Data file. **j**, Comparative binding showed that the furan ring of SalA, the phenylalanine residue of dynorphin A<sub>1-13</sub>, the iodobenzene ring of MP1104 and the furan ring of nalfurafine are overlapped in the extended hydrophobic pocket formed by W124<sup>ECL1</sup>, V134<sup>3,28</sup>, and I135<sup>3,29</sup>. **k**, Structural comparison of the hydrophobic pocket encapsulating the acetyloxy group of SalA, with corresponding binding regions of nalfurafine and MP1104.

**Fig. 3 | The lipid-mediated interface of  $\kappa$ OR dimer. a-b**, Cryo-EM density map produced by post-processing (**a**) and structural model (**b**) of  $\kappa$ OR dimer. Purple density represents cholesterol (CLR), grey density represents C16:0 fatty acids (PLM) and blue density represent cholesteryl hemisuccinate (CHS). **c**, Schematic representation of the NanoBiT design principle. **d-g**, The TM1, TM2 and Helix 8 interface of  $\kappa$ OR extracellular region. NanoBiT curves of LgBiT- $\kappa$ OR with different quantity of WT and mutations of SmBiT- $\kappa$ OR. RLU, relative luminescence units. Data were normalized to WT and shown as mean  $\pm$  S.E.M. from at least three independent biological triplicates ( $n=4$  for WT and  $n=3$  for mutants) each performed in triplicates. (**d**) displayed the amino acids on TM1 that were near the extracellular side and involved in CHS and CLR mediated TM1-TM1 interactions. (**e**) displayed the amino acids on TM1 that were near the intracellular side and involved in PLM, CLR and CHS mediated TM1-TM1 interactions. (**f**) displayed the amino acids on TM2 that were near the extracellular side and involved in CHS and CLR mediated TM2-TM2 interactions. (**g**) displayed the amino acids on Helix8 and involved in Helix8-Helix8 interactions. Combo indicates the combination of V75A/F341A/F346A. Note: The numerical data with statistics of titration assay is shown in Supplementary Table 3. Source data are provided as a Source Data file. **h**, NanoBiT luminescence measurements of WT  $\kappa$ OR dimers following treatment with increasing concentrations of methyl- $\beta$ -cyclodextrin (M $\beta$ CD), showing a significant reduction in dimer signal upon cholesterol depletion. Data shown are mean  $\pm$  S.E.M. from three independent biological replicates, each performed in technical triplicates. The significance was analyzed using one-way ANOVA with a Dunnett's multiple comparisons test (two-sided). ( $P=0.3598$ ,  $P=0.2624$  and  $P=0.0133$  from left to right). \* $P < 0.05$ ; ns, not significant  $P > 0.05$  vs. 0 mM MCD treatment. Source data are provided as a Source Data file. **i**, Close-up view of the cholesterol (purple) binding site at the  $\kappa$ OR dimer interface, highlighting residues that form direct contacts with cholesterol in

the cryo-EM structure. **j.** NanoBiT luminescence measurements of  $\kappa$ OR cholesterol-interaction mutants following M $\beta$ CD treatment, showing no significant change in dimer signal across concentrations. Data are mean  $\pm$  S.E.M. from three independent experiments performed in technical triplicates. ( $P=0.7404$ ,  $P=0.9305$  and  $P=0.6221$  from left to right. The statistical test used was one-way ANOVA with a Dunnett's multiple comparisons test). ns, not significant  $P > 0.05$  vs. 0 mM MCD treatment.

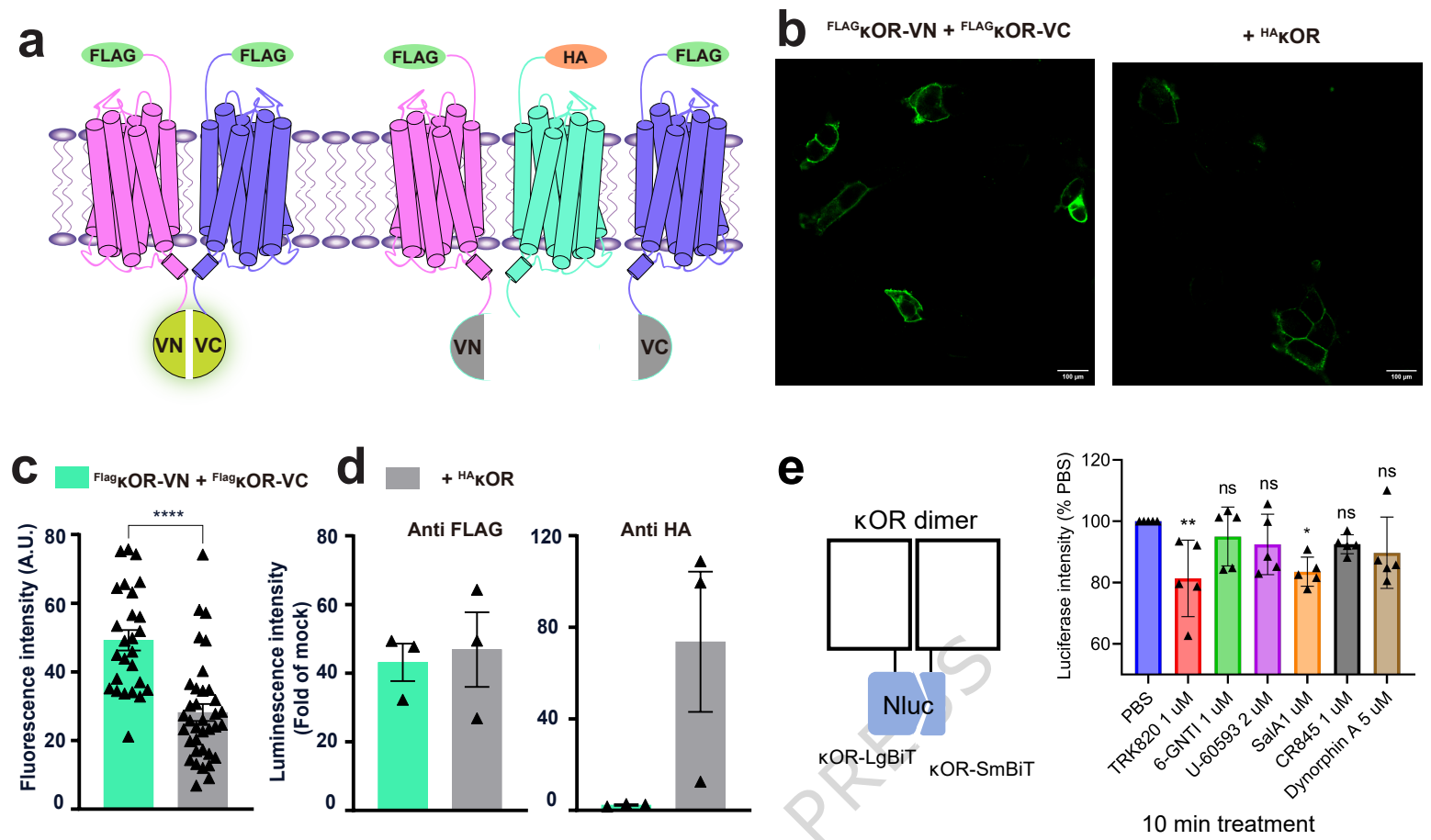
**Fig. 4 |  $\kappa$ OR dimerization enhances G protein signal.** **a,** Blots showing cross-linking of the cell surface  $\kappa$ OR between the indicated residues mutated into cysteine (Cys), in the indicated TM helices, without or with CuP. Data are mean  $\pm$  S.E.M. from four independent biological replicates and analyzed using one-way ANOVA with a Dunnett's post-hoc multiple comparison test to determine significance: compared with WT CuP +, \*\*\*\* $P < 0.0001$ , \*\*\* $P < 0.001$ , \*\* $P < 0.01$ . ( $P < 0.0001$ ,  $P < 0.0001$ ,  $P = 0.0011$ ,  $P = 0.0002$ ,  $P < 0.0001$ ,  $P < 0.0001$  and  $P < 0.0001$  from left to right). Source data are provided as a Source Data file. **b,** Characterization of ligand affinity for  $\kappa$ OR dimer interface mutants by radio-ligand competition binding assays. Data are mean  $\pm$  S.E.M. from three independent biological replicates. Source data are provided as a Source Data file. **c,** Cell surface expression of  $\kappa$ OR WT and the indicated mutants detected by ELISA. Data are mean  $\pm$  S.E.M. from three independent biological replicates each performed in triplicates, and analyzed using one-way ANOVA with a Dunnett's post-hoc multiple comparison test to determine significance: compared with WT, not significant (ns)  $P > 0.05$ . ( $P = 0.1962$ ,  $P = 0.2001$ ,  $P = 0.9305$  and  $P = 0.5737$  from left to right). Source data are provided as a Source Data file. **d,**  $G_i$  protein activation of  $\kappa$ OR WT and the indicated mutants with CuP treatment upon SalA stimulation. Data are mean  $\pm$  S.E.M. from at least three independent biological replicates ( $n=6$  for WT and  $n=3$  for mutants) each performed in triplicates. Source data are provided as a Source Data file. **e,** The  $E_{max}$  and  $pEC_{50}$  of SalA in  $\kappa$ OR WT and the indicated mutants in (d). Data are presented as mean  $\pm$  S.E.M. from at least three independent experiments ( $n=6$  for WT and  $n=3$  for mutants) performed in triplicates. Data are analyzed using one-way ANOVA with a Dunnett's post-hoc multiple comparison test to determine significance: compared with WT, \*\*\*\* $P < 0.0001$ , \*\*\* $P < 0.001$ , \* $P < 0.05$ ; ns, not significant  $P > 0.05$ .  $E_{max}$  ( $P = 0.4374$ ,  $P < 0.0001$ ,  $P = 0.0127$ ,  $P = 0.0008$  from left to right).  $pEC_{50}$  ( $P = 0.7562$ ,  $P = 0.0317$ ,  $P < 0.0001$  and  $P < 0.0001$  from left to right). Source data are provided as a Source Data file. **f,** Schematic presentation of BRET assay measuring G protein recruitment to  $\kappa$ OR dimer, which is formed by fusing LgBiT and HiBiT in the C-terminus. **g,** SalA-induced G protein recruitment to dimeric  $\kappa$ OR WT or  $\kappa$ OR dimer with R156<sup>3.50</sup>A mutation. Data are presented as means  $\pm$  S.E.M. from four independent biological replicates respectively, each performed in triplicate. Source data are provided as a Source Data file.

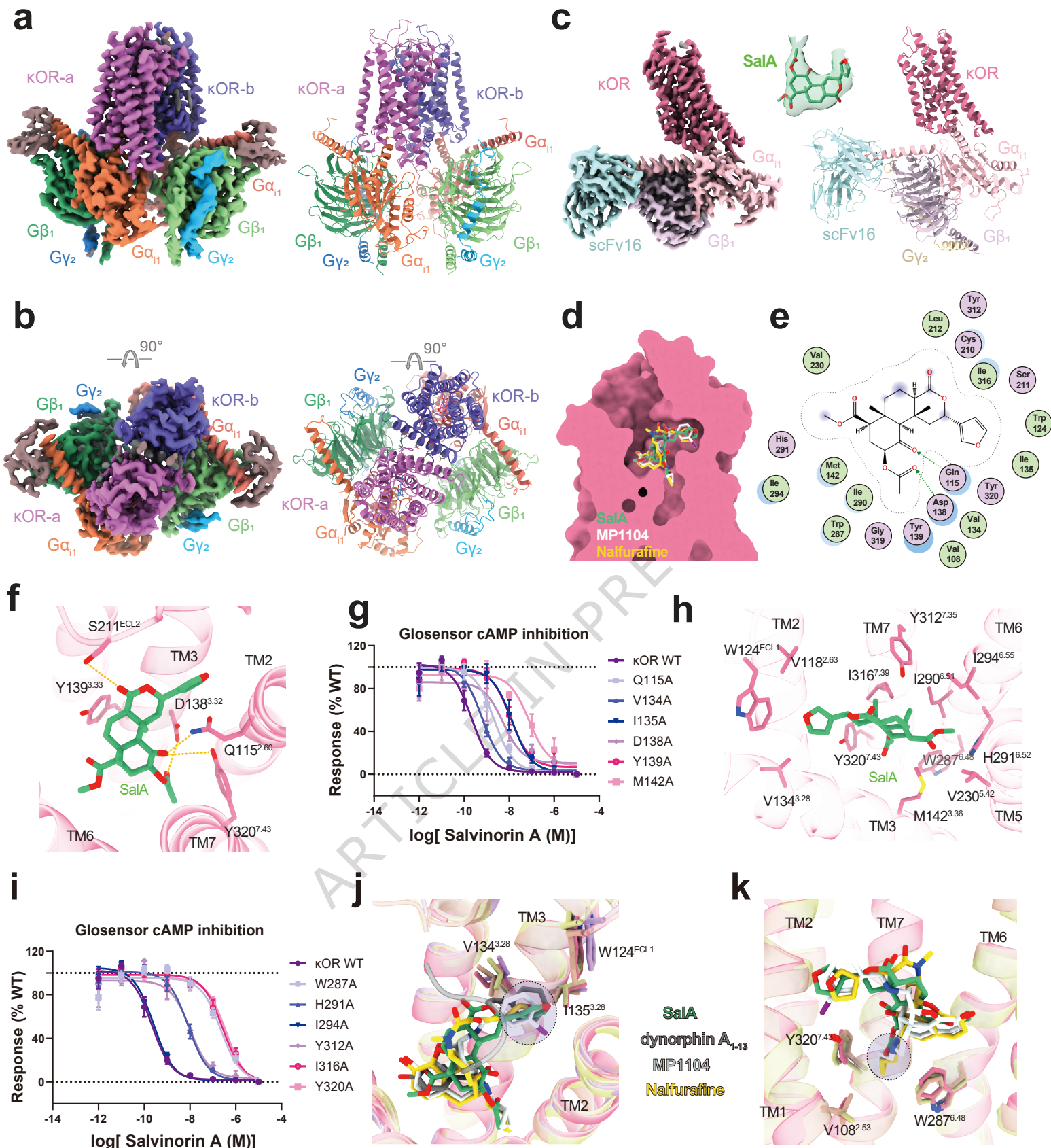
**Editorial Summary:**

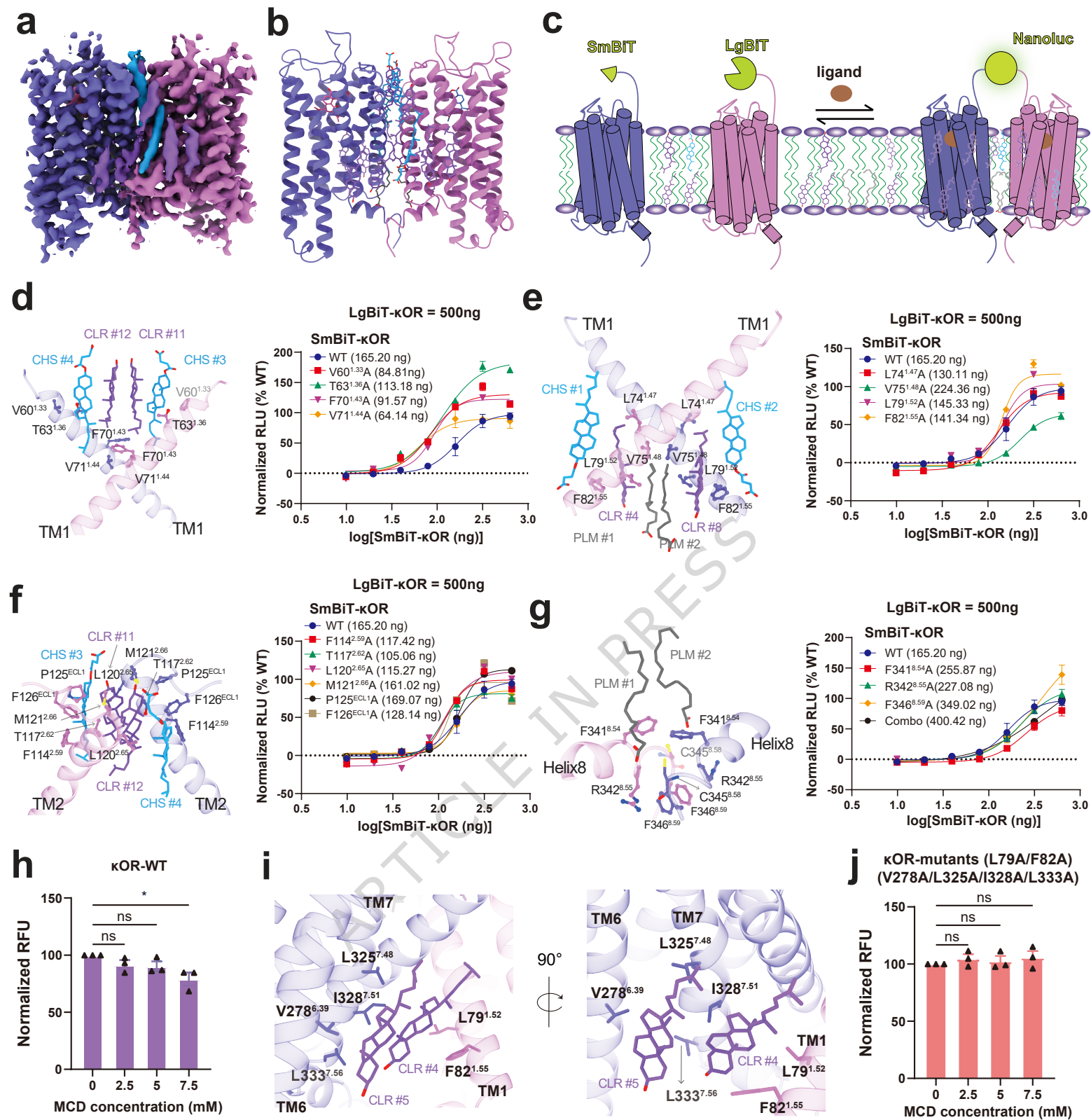
The  $\kappa$ -opioid receptor ( $\kappa$ OR) is a promising target for safer pain therapies. Here, authors present the cryo-EM structure of a salvinorin A-bound  $\kappa$ OR dimer complexed with two  $G_i$  proteins, revealing a lipid-mediated interface and dimerization-enhanced  $G_i$  recruitment.

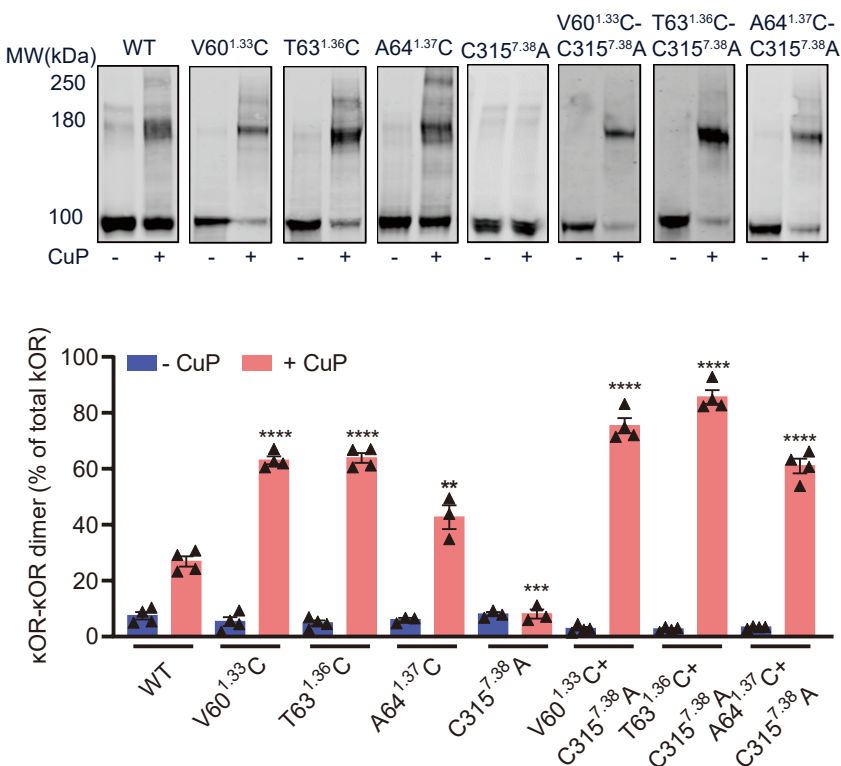
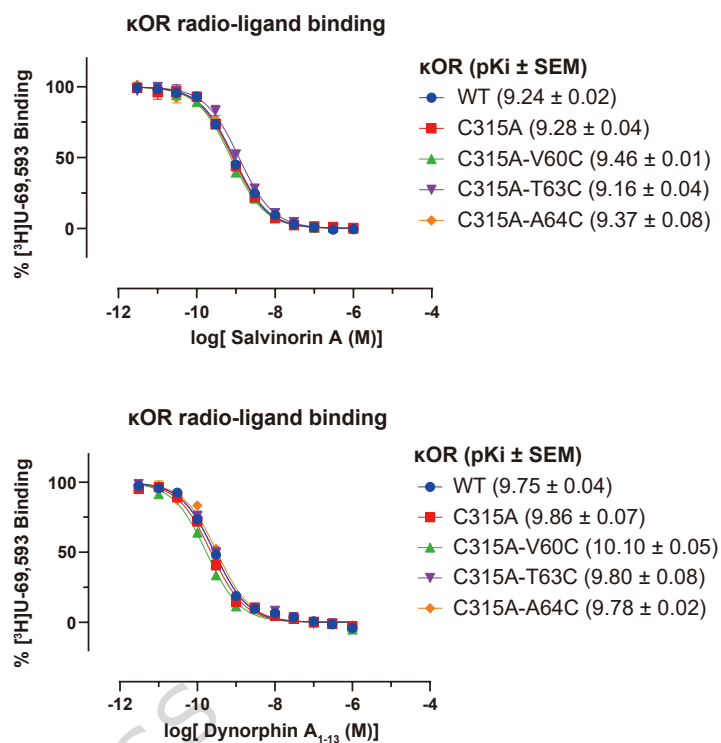
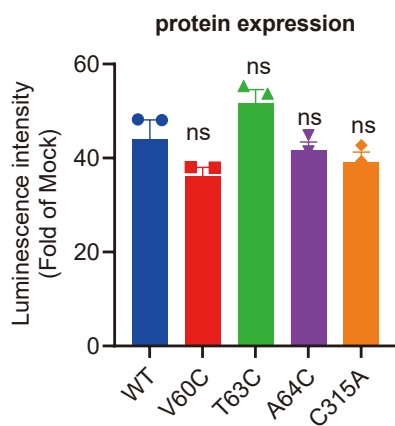
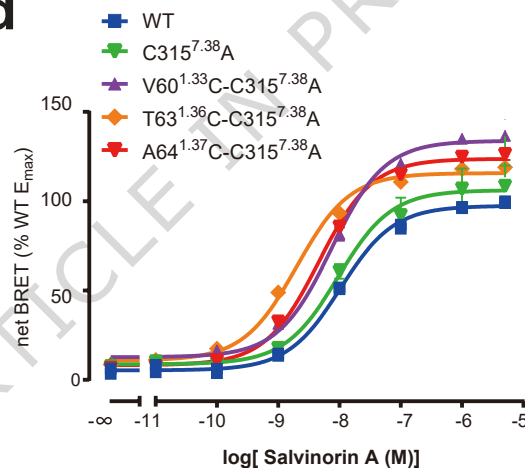
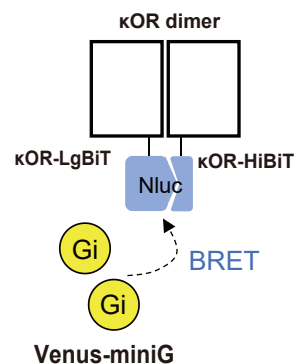
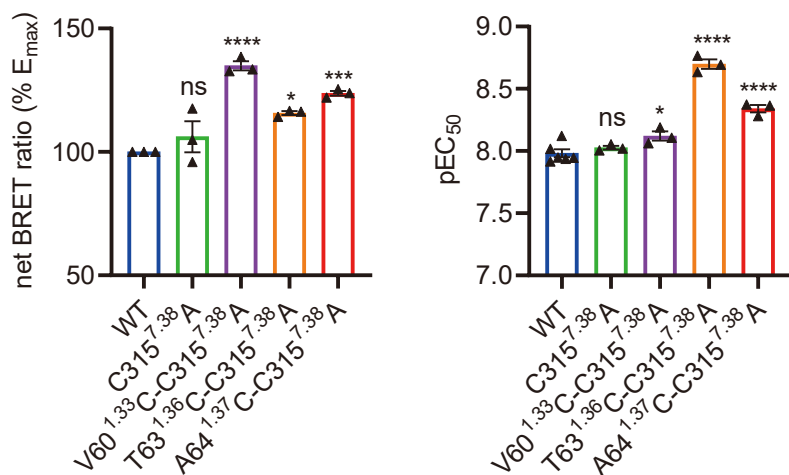
**Peer review information:** *Nature Communications* thanks Kirill Martemyanov and the other, anonymous, reviewer(s) for their contribution to the peer review of this work. A peer review file is available.

ARTICLE IN PRESS







**a****b****c****d****f****e****g**